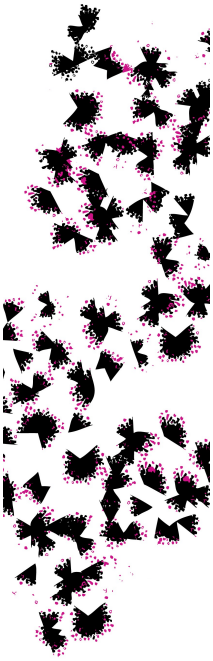

Design of a test setup for the Robird

M.C. (Cham) Bustraan

BSc Report

Committee:
Prof.dr.ir. S. Stramigioli
Dr.ir. G.A. Folkertsma
W. Straatman, MSc
Dr.ir. W.B.J. Hakvoort

July 2018

020RAM2018
Robotics and Mechatronics
EE-Math-CS
University of Twente
P.O. Box 217
7500 AE Enschede
The Netherlands

Design of a test setup for the Robird

Cham Bustraan

July 4, 2018

Abstract

In the report a test setup was made for the Robird using parallel leaf springs. The goal was to design it in such a way that when placed in a wind tunnel the Robird would be kept in place but would other oscillate and pitch at it would during actual flight. Two prototypes were designed, the second a lighter version of the first, and both showed a response similar to the mathematical model made. Time of Flight sensors were to be used to measure the displacement of the Robird's body and while these operational they cannot yet be implemented properly. The prototypes made serve as a proof of concept, but more work needs to done on making the setup lighter, investigating the pitching motion, and implementing the sensors.

Contents

1 Introduction **1**
1.1 Previous designs 1
1.2 Goal of this bachelor assignment 1

2 Requirements and concept sketch **3**
2.1 Requirements 3
2.2 Concept sketch 4

3 Mathematical Analysis **5**
3.1 Leaf springs 5
3.2 Analysis of the motion 5

4 Dimensioning **14**
4.1 Leaf spring dimension determination 14
4.2 Distance between front and back springs 17

5 Design **19**
5.1 Block design 19
5.2 Sensor investigation 22

6 Testing **24**
6.1 Test method 24
6.2 Results 24

7 Discussion **30**
7.1 Problems 30
7.2 Improvements 31

8 Conclusion **34**

A Appendix: Final versions of individual plates **35**
A.1 Side block 35
A.2 Top Block 36

B Appendix: Other data gathered **38**
B.1 Oscillation 38
B.2 Pitching 40
B.3 Side Blocks 43

Bibliography **44**

1 Introduction

There have been 65 139 reported bird strikes between 2011 and 2014 (Seidenman, 2016) and the annual costs due to damage and delays of commercial aircrafts is estimated to be 1.28 billion US dollars (Allan and Orosz, 2001). Due to the financial and bird life loss many methods have been employed to reduce the risk of a collision between a bird and an aircraft such as ridding the surrounding area of crops, or through the use of explosives, cannons or fireworks (Rosenberg, 2017). However, birds are intelligent creatures and will soon realize that there is no real threat. Some airports utilize the use of a natural predator such as a falcon to scare the other birds but these require care, food, and rest and cannot herd birds in a certain direction. There is also the risk that the falcon will push birds into an aircraft's path or go there itself. For this reason, Clear Flight Solutions has designed the Robird, a remotely controlled robotic bird. Through a combination of silhouette and wing movement the Robird triggers the instinct of birds making the chasing off of birds fully controllable.

The Robird's initial flight mechanism was made through a process of trial and error since little is known about how birds are capable of flight. Hence, it isn't entirely understood why the Robird flies either. However, now that the Robird is operational and employed commercially we are capable of studying the Robird's motion in an effort to understand the flight of birds and improve the design of Robird through this. Currently there are only two methods of testing available: placing a single wing in a wind tunnel, and actually flying the Robird in the open air. The first method is insufficient if one wants to know the behavior of the complete Robird. As the Robird must be very lightweight to be able to fly it is difficult to attach sensors to it. This makes data collection difficult during flight and there is the risk of damaging the Robird. As such there is a need for a dynamic test setup for the entire Robird which can be placed in a wind tunnel and from which data can be collected to determine its lift, pitch, roll, and other features.

1.1 Previous designs

Two years ago Erik Landman also had the assignment to construct a test setup would allow the Robird to mimic real flight for testing and flight analysis purposes. In his report he discussed many different possible designs, but finally decided to create a setup based on Evans four-bar approximate straight line mechanism (Landman, 2016). While his design was well thought out, with a focus on a good pitching response, the main flaw of the setup was that it exhibited resonance within the operating frequencies of the Robird and wasn't capable of adequately compensating for its gravitational load. Beyond that there were a few minor flaws such as wings hitting the table during operation, and a lack of sensors on the setup itself.

1.2 Goal of this bachelor assignment

The goal of this bachelor assignment is the design of a new test setup for the Robird. Erik Landman's work serves as a good foundation for design considerations and pitfalls to watch out for. A significant difference between this new setup and the old is that new setup will be built for the explicit purpose of placing it and the entire Robird in a wind tunnel during operation.

To begin with, the necessary requirements for the test set-up will be determined and a concept sketch will be presented and explained. Following this, a mathematical analysis of the setup will be carried out. This analysis will then be used to determine the exact dimensions of the springs. Once these are known the details of the design will be made and the first prototype constructed. This prototype will then be tested to validate the design choices made based on the mathematical analysis, whereupon a new design will be made and tested to improve the frequency response of the setup.

The thesis is structured as followed. Chapter 2 will cover the requirements and concept sketch of the setup. In chapter 3 the mathematical analysis will be shown. The determination of the setup dimensions will be done in chapter 4. The specific design and sensor implementation will be presented in chapter 5. Chapter 6 will discuss the method of testing and include the results. The discussion can be found in chapter 7, and the conclusion in chapter 8.

2 Requirements and concept sketch

2.1 Requirements

While the setup has yet to be designed it is known what specifications it should adhere to. Chief of these is that the motion of the Robird's body should be as realistic as possible within its operating frequencies. The body of the Robird in flight is expected to have an oscillation amplitude of about 1.5 cm, and operates at a frequency between 4 and 6 Hz for steady flight. To make the testing in the wind tunnel as realistic as possible it is desirable that within this frequency range the the motion of the Robird is not affected by the setup. A similar requirement exists for the pitching of the Robird. Another such requirement could be set for the roll of the Robird, however, this is not as critical as the oscillation and the pitching so it will only be looked at if time allows and if it does not conflict with other requirements. These are the primary requirements for the setup to be successful but they need to be quantified such that they provide boundaries for the design. Therefore, the complete list of requirements is given in table 2.1, with an elaboration included below.

Subject	**Requirement**
x- and y-direction	Fixed
z-direction	Oscillation within boundaries
θ- and Φ-rotation (pitch and roll)	Possible
ψ-rotation (yaw)	Fixed
Behavior within operating frequencies of 4 to 6 Hz	Max 5 dB offset from free mass oscillation and pitch
Minimum possible body displacement in z	2.5 cm
Maximum dimensions	0.2 m×0.5 m×0.2 m (x,y,z)
Maximum additional mass added to Robird	70 g
Measurements	displacement in z-direction at two points along x-axis

Table 2.1: Requirements for the test setup

The axes and rotation directions stated in table 2.1 are shown in the concept sketch in figure 2.1. For the motion in the z-direction by 'Oscillation within boundaries' is meant that while the Robird should act as naturally as possible the setup should prevent it from moving too much, such as breaking off from the setup and flying away. For reasons that will be explained in chapter 3 the oscillation and pitch of a free mass is an asymptote that the system will tend towards as frequency increases. While it is desirable to have as little difference as possible between these two lines, to quantify this a maximum difference of 5 dB was chosen. While it was mentioned above that the oscillation of the Robird's body is expected to be 1.5 cm for the sake of security and to accommodate possible pitching, it was decided that the setup should be stable and predictable for deflections at least up to 2.5 cm. To prevent the setup from becoming impractical in size this has been restricted to at most 0.2 m in and the x- and z-direction and 0.5 m in the y-direction. For the Robird to be able to generate lift, its weight combined with its connection

to the setup should be minimized. As long as this additional weight is below 70 g then it should be able to generate enough lift to fly.

2.2 Concept sketch

To follow the above requirements a setup is needed that only allows for easy movement in one direction and two rotations. In the Erik Landman's bachelor he considered a number of options for possible designs including: a moving platform, direct constraint, double vertical guides, and Evans straight line mechanism (Landman, 2016). While his research was thorough and well thought out, he did not consider the possibility of using leaf springs as opposed to linear springs.

A leaf spring is nothing more than a thin sheet of material which can act as a linear spring within a certain deflection range from its neutral position. Leaf springs will be discussed in more detail in chapter 3 but a key property they have is that if a leaf spring is placed lengthwise along the y-axis then its stiffness in the x- and y-direction is much greater than that in the z-direction. Therefore, if placed in the right orientation these can restrict the desired degrees of freedom while allowing for oscillation in the others.

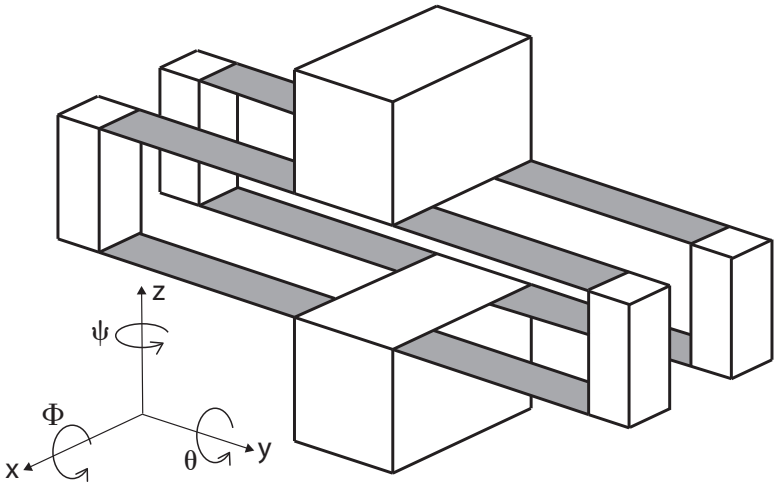

Figure 2.1: Rough sketch of test setup.

A rough sketch of an envisioned test setup is shown in figure 2.1. The areas in grey are leaf springs and the white blocks are rigid bodies. The Robird is fixed to the top block with its length along the x-axis while the bottom block is fixed to the ground. By orienting the leaf springs in this way the bending in the z-direction can be made to match the design requirements while keeping the stiffness in the other direction much greater, effectively preventing movement in those. It was chosen to use four sets of parallel leaf springs for a number of reasons. First, it allows for pitching to be controlled through the separation between the front and back springs. Second, the symmetry of the setup should prevent the Robird from moving in an arc. The decision to use parallel leaf springs rather than a single leaf spring of twice the length was made to allow for a low net spring constant, while staying within the physical boundaries of the setup.

As the Robird moves, the body's oscillation occurs the z-direction, pitch is the θ rotation, and roll is the Φ rotation. Data can collected by measuring the distance between the top and bottom block at various points. Together with the stiffness of the parallel springs one can also determine forces acting on the Robird body. Through the net displacement of the top block the lift force can be determined. Pitch can be determined through the difference in displacement of the front and back of the top block.

3 Mathematical Analysis

This chapter will discuss the theoretical foundation required for the determining the dimensions of the setup shown in figure 2.1. This includes covering the working principles behind leaf springs, applying these concepts to the test setup, and deriving equations which can be used to determine the dimensions of the leaf springs.

3.1 Leaf springs

As was mentioned in chapter 2 leaf springs act as linear springs as long as the plate is not plastically deformed and deflections are small relative to its length. As the leaf springs will be clamped on both their ends their bending shape is what's known as an s-shape bending mode. In figure 3.1 the bending shape of the leaf springs for the z-direction oscillation of the test setup can be seen for clarity.

Figure 3.1: Bending shape for double clamped leaf spring.

The bending shape has a large effect on the stiffnesses of the plate. The equation for the translational and rotational spring constants for a single leaf spring bending, following the axes of figure 3.1 are given below (Janssen Precision Engineering, 2018):

$$k_x = \frac{Etb^3}{4L^3} \qquad k_y = \frac{Ebt}{L} \qquad k_z = \frac{Ebt^3}{L^3} \tag{3.1}$$

$$k_\Phi = \frac{Ebt^3}{12L} \qquad k_\theta = \frac{Gbt^3}{3L} \qquad k_\psi = \frac{Etb^3}{12L} \tag{3.2}$$

Where $k_{x,y,z}$ is the lateral bending stiffness in $\mathrm{N\,m^{-1}}$, $k_{\Phi,\theta,\psi}$ is the torsional bending stiffness in $\mathrm{N\,m\,rad^{-1}}$, E is the Young's modulus in $\mathrm{N\,m^{-2}}$, G is the shear modulus in $\mathrm{N\,m^{-2}}$, and b, L and t are the dimensions of the plate in the x, y, and z directions respectively, given in meters. Based on these equations one can see that the stiffness k_z is typically small compared to k_x and k_y given that the length of the plate L is greater than the width b which in turn is greater than the thickness t. For instance, if $L = 10b = 100t$ then $k_y = 400k_x = 10000k_z$. It for this reason that their use is ideal to make a test setup for the Robird.

3.2 Analysis of the motion

The test setup is nothing more than four sets of leaf springs connected to a single mass in parallel. These sets of leaf springs can be seen as two springs which are connected in series through a rigid body. The other ends are connected to ground and the top block. The motion of the test setup and the Robird can be split in two: the whole oscillation of the Robird body, and the

pitching of the Robird. The goal of this analysis is to derive a method for determining what spring constant the leaf springs should have and how far apart the front and back sets should be. To this end a few assumptions will be made of which the validity range will be discussed in subsection 3.2.4. The assumptions are as followed:

- The leaf springs always act as linear springs, and never plastically deform or fatigue.
- All motion of the top block in the y-direction is negligible.
- During flight in the wind tunnel the Robird will compensate for its own gravity through the generated lift so it does not have to be included in the model.
- The mass of the side blocks is considered negligible compared to the combined mass of the top block and the Robird.

3.2.1 Parallel spring simplification

Using the above mentioned assumptions the top and side blocks may be considered to be simple guided supports with the side block guiding both leaf springs. This is shown schematically in figure 3.2.

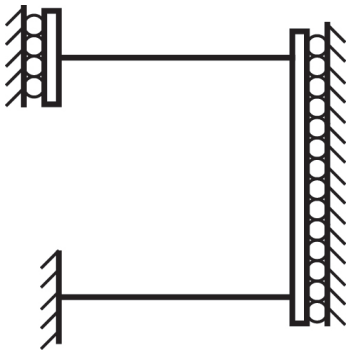

Figure 3.2: simplification of parallel spring system.

When deflections are considered small, leaf springs produce a force which is proportional to its deflection. In this way they are identical to regular springs and can be modeled as such. This means that figure 3.2 can also be seen as two linear springs in series, as the end of one leaf spring is rigidly connected to the other. It is well known that for springs in series the total equivalent spring constant is given by:

$$\frac{1}{k_{eq}} = \frac{1}{k_1} + \frac{1}{k_2} \tag{3.3}$$

$$k_{eq} = \frac{k_1 k_2}{k_1 + k_2} \tag{3.4}$$

As both leaf springs will be of identical dimensions their stiffness will be the same, so $k_1 = k_2$. As stated in (3.1) the spring constant of these springs is given by:

$$k_z = \frac{Ebt^3}{L^3} \tag{3.5}$$

Combining (3.5) and (3.4) an equivalent stiffness k_{eq} for the the parallel leaf springs can be determined.

$$k_{eq} = \frac{k_z^2}{2k_z} = \frac{Ebt^3}{2L^3} \tag{3.6}$$

So a set of parallel springs can be reduced to a single spring with half the stiffness and there are four of these connected to the top mass, two in the front and two in the back.

3.2.2 Robird oscillation

For the moment it is assumed that the Robird's body does not pitch and is simply oscillating up and down due to the movement of the wings. In this case all of the springs supporting the Robird will have the same deflection and therefore their spring constant may be summed together into one single spring. The the oscillation of the Robird may therefore be modeled as a simple mass-spring system with a harmonic force applied to the mass. A schematic drawing and free body diagram of this motion is shown in figure 3.3.

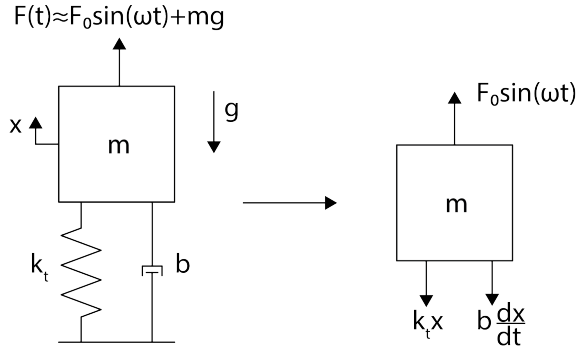

Figure 3.3: Schematic drawing and free body diagram of simplified oscillation motion.

The general transfer function, including damping, for relating the force applied to the displacement of the mass for such a system is well known and given below:

$$\frac{X(s)}{F(s)} = H(s) = \frac{1}{ms^2 + bs + k_t} = \frac{K\omega_n}{s^2 + 2\zeta\omega_n s + \omega_n^2} \tag{3.7}$$

Where m is the combined mass of the Robird and the top block, ζ is the damping coefficient, and $k_t = 4k_{eq}$ is the total spring constant of the four parallel leaf spring sets. This system therefore has resonance frequency, ω_n, of $\sqrt{k_t/m}$ and a steady state gain, K, of $1/k_t$. As the mass of the Robird is known, m is also approximately known and constant. The goal is find a k_t such that the response within the operating frequency of the Robird is like that of a freely oscillating mass. This can be found by looking at the bode plot of the system. The bode plot of such second order transfer function has the general form given in figure 3.4.

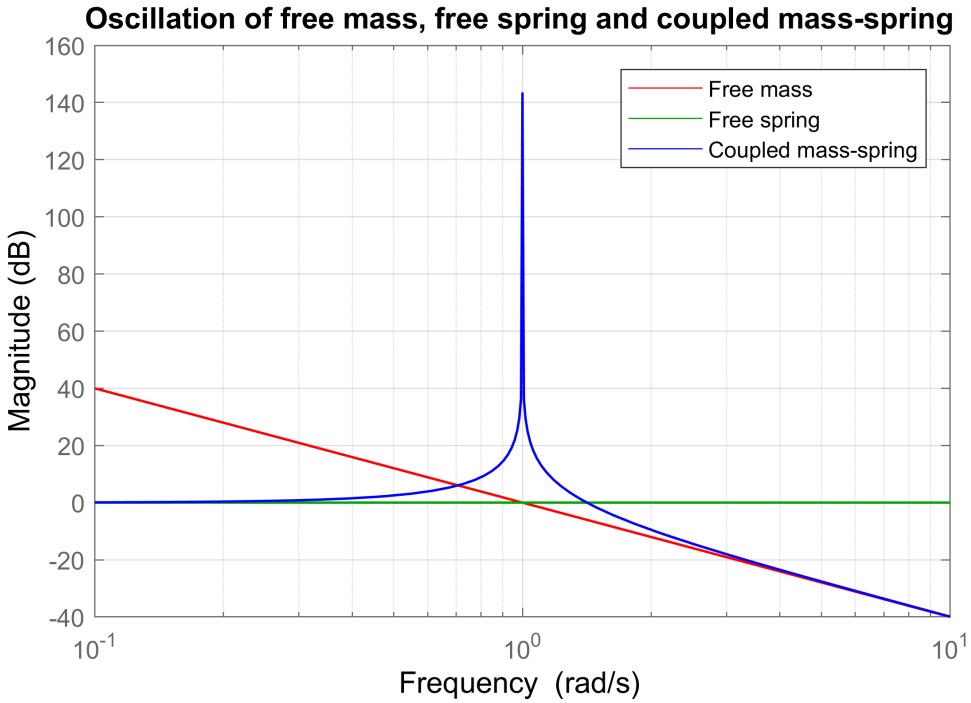

Figure 3.4: General bode plot for a second-order system. In the figure itself both the mass and the spring constant were set to 1 with no damping to display the general behavior. For the Robird's oscillation steady-state gain $K = 1/k_t$ and resonance frequency $\omega_n = \sqrt{k_t/m}$. For the Robird's pitching $K = 1/4\left(k_{\theta eq} + k_{eq}r^2\right)$ and $\omega_n = \sqrt{4\left(k_{\theta eq} + k_{eq}r^2\right)/J}$.

As can be seen the bode plot of just a spring is a horizontal line and the bode plot of a free mass is a line whose transfer decreases at a rate of 40 dB per decade. We can also see that for a mass-spring system the transfer function is combination of these two behaviors with resonance occurring at the intersection. Therefore, if the resonance frequency of the test setup is made to be lower than the operating frequency range the setup should allow for the Robird to move as it would in real flight.

3.2.3 Robird pitching

In a similar manner to the Robird's oscillation, by examining the Robird's pitching it will be determined what the distance between the front and back springs should be. In this case we consider the Robird as a mass with a moment of inertia about the y-axis, J, with a moment applied at the Robird's center of mass due to its pitching. At a distance r from this the center of mass in both directions are springs each with a spring constant of $0.5k_t$, or $2k_{eq}$. As the Robird begins to pitch one spring will be extended, while the other compresses, countering the applied moment. In addition this as the Robird pitches the springs will twist as well, generating another moment with spring constant $k_{\theta eq} = k_\theta/2$ per parallel spring set. A schematic drawing of this motion can be seen in figure 3.5.

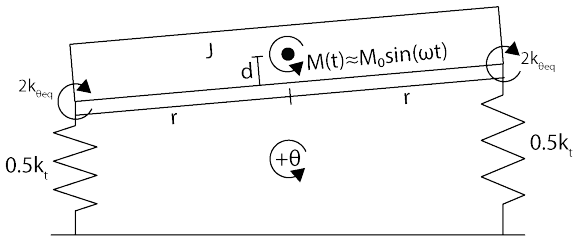

Figure 3.5: Schematic drawing of the pitching motion.

Under the small angle approximation this system is a linear second order system with the following transfer function:

$$G(s) = \frac{1}{J\left(s^2 + 2s\zeta\sqrt{\frac{4(k_{\theta eq}+k_{eq}r^2)}{J}} + \frac{4(k_\theta+k_{eq}r^2)}{J}\right)} \tag{3.8}$$

$G(s)$ will have same general shape as shown in figure 3.4 but the parameters are different compared to the case of the Robird's oscillation. The steady state gain is $\frac{1}{4(k_{\theta eq}+k_{eq}r^2)}$ and the resonance frequency is $\sqrt{\frac{4(k_{\theta eq}+k_{eq}r^2)}{J}}$. As J is a property due to the Robird's shape and mass, it is constant. k_t will be determined through the Robird's oscillation and k_θ also follows from the dimensions of the leaf spring so the distance to the center is the one parameter left that can be changed. The Robird should have a natural pitching behavior in its operating frequencies when these frequencies are after the resonance peak. The pitching behavior of the setup will be determined by choosing r such that the pitching behavior is within 5 dB of the the Robird's free pitching motion.

3.2.4 Validity range of assumptions

In the beginning of this section a number of assumptions were listed. It is important to examine what makes these reasonable assumptions and under what conditions they hold as this could restrict the design choices available. The assumptions will be examined in the same order as they were listed above.

The leaf springs always act as linear springs, and never plastically deform or fatigue

It is known that for small deflections a spring behaves linearly. In order to design a test setup that stays within this linear range, it is important to know how great the deflection relative to the spring's length is allowed to be. It is also important to ensure that the maximum stress on the leaf is low enough so as not to cause plastic deformation or fatiguing over time.

According to Soemers (2011) on the subject of position dependent parallel flexure guiding the displacement in the z-direction will only slightly affect the stiffness in the z-direction. It goes on to give the example that for $\Delta z/L = 0.22$ the stiffness is increased by 5% and that this is due to "geometric non-linearity". Hence 22% of a leaf spring length will be taken the allowable deflection limit for the assumption of linear deflection behavior to hold.

For k_θ no information can be found pertaining to the influence of Δz on its value. It will be assumed that its change is also negligible for a deflection 22% of its length.

The maximum stress exerted on an s-shape leaf spring is given by (Janssen Precision Engineering, 2018):

$$\sigma_{max} = \frac{FLt}{2I} = \frac{3Et}{L^2} z_{max} \tag{3.9}$$

When determining the dimensions of the plates it must ensured that the maximum predicted stress is below the maximum stress of the material before plastic deformation or fatiguing occurs and that its length is long enough relative to the maximum deflection such that the leaf spring remains linear.

All motion of the top block in the y-direction is negligible

Due to the symmetry of this setup the top block should be pulled to each side equally as it moves, eliminating the effect and keeping the movement straight.

Motion to the left and right of the top block can still occur if a force in the direction is applied to it as this would need to be counteracted by the k_y of the upper springs and k_Φ of the lower springs. As $k_y \ll k_\Phi$ it is possible that if k_Φ is not great enough that the Robird does have some freedom in this direction. Forces that could cause this behavior are not expected, since even during a roll forces would be applied in the z-direction the springs for small angles. Even potential significant forces in the y-direction during roll shouldn't cause movement in that direction as they are opposite and equal on either side block. Movement in the direction could only occur if all parallel leaf spring sets experience a force in the same direction, which is deemed highly unlikely.

During flight in the wind tunnel the Robird will compensate for its own gravity

As long as the Robird is lightweight enough and has forward velocity relative to the air around it, it can generate enough lift to keep itself in the air during real flight. With the Robird kept in place and wind applied against it in a wind tunnel the same effect should occur. This is why it is essential that the additional effective weight of the test setup is not too great. It also means that the setup is of no use outside a wind-tunnel, and a foam block or such is necessary for the Robird to rest on outside of operation. During start-up the Robird will need to pass through the resonance frequency but this is an effect that can't be helped and it should pass through this frequency quickly.

It is also possible that the presence of the test setup influences the flow around the Robird in such a way that it can longer generate lift. For now the assumption is made that this is not case, but to be sure the behavior of the air around the setup should be investigated but is beyond the scope of this assignment.

The mass of the side blocks is considered negligible

If the mass of the side blocks were not negligible then it would be as seen in figure 3.6. Now the effect of this m_2 will be investigated.

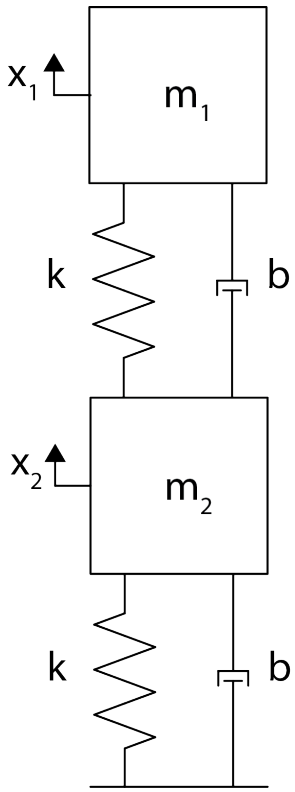

Figure 3.6: Schematic drawing of double mass oscillation motion.

In this case the oscillation motion will have the following transfer function:

$$\frac{X_1(s)}{F(s)} = H(s) = \frac{m_2 s^2 + 2bs + 2k}{m_1 m_2 s^4 + (2m_1 + m_2)\, bs^3 + \left((2m_1 + m_2)\, k + b^2\right) s^2 + 2bks + k^2} \tag{3.10}$$

Due to the presence of the secondary mass a second resonance peak will be observed as well as an anti-resonance drop in between these peaks. The heavier the mass of this secondary mass is the closer these two peaks will be. Hence, if the secondary mass is too great then this could interfere with the response within the operating frequencies. There is also the additional problem of the the gravity compensation due to lift becoming more challenging if the secondary masses become too heavy.

To determine the maximum mass that all four side blocks in total are are allowed to be the spring constant per leaf spring as determined in chapter 4 is used in conjuction with the Robird mass of 0.8 kg as m_1 and m_2, the total side block mass, is varied as fraction of m_1. The method does rely on the assumption that all four side blocks move in the same way throughout the oscillation. The general result can be seen in figure 3.7 and the result zoomed into the operating frequency range is shown in figure 3.8.

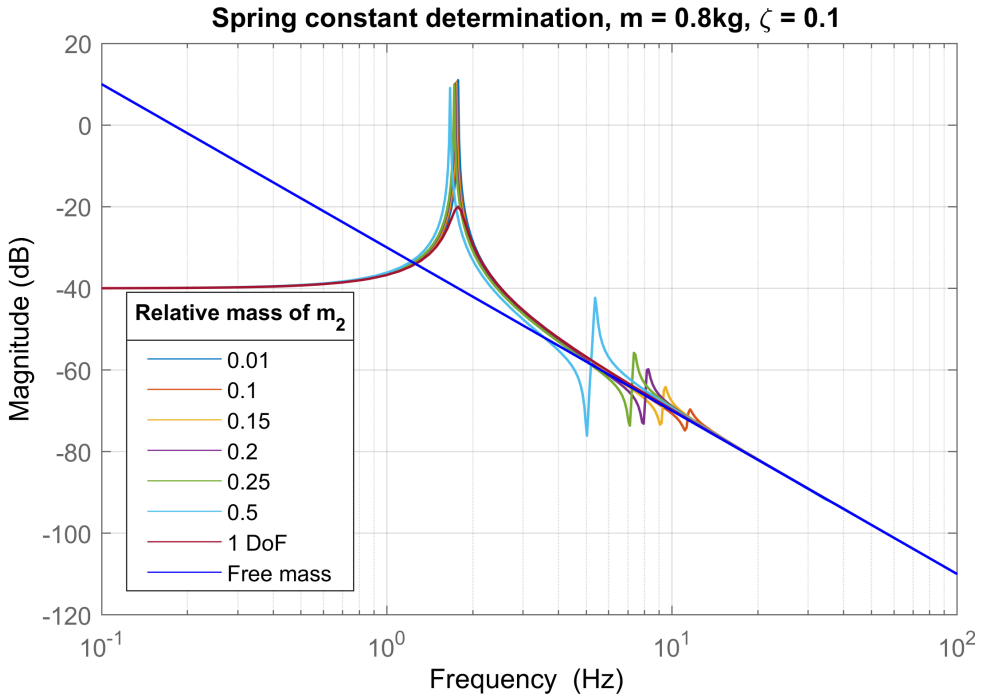

Figure 3.7: Effect of secondary mass relative to primary mass using spring constants found in chapter 4. The viscous damper constant, b, has been set to 0.1 $\mathrm{N\,s\,m^{-1}}$.

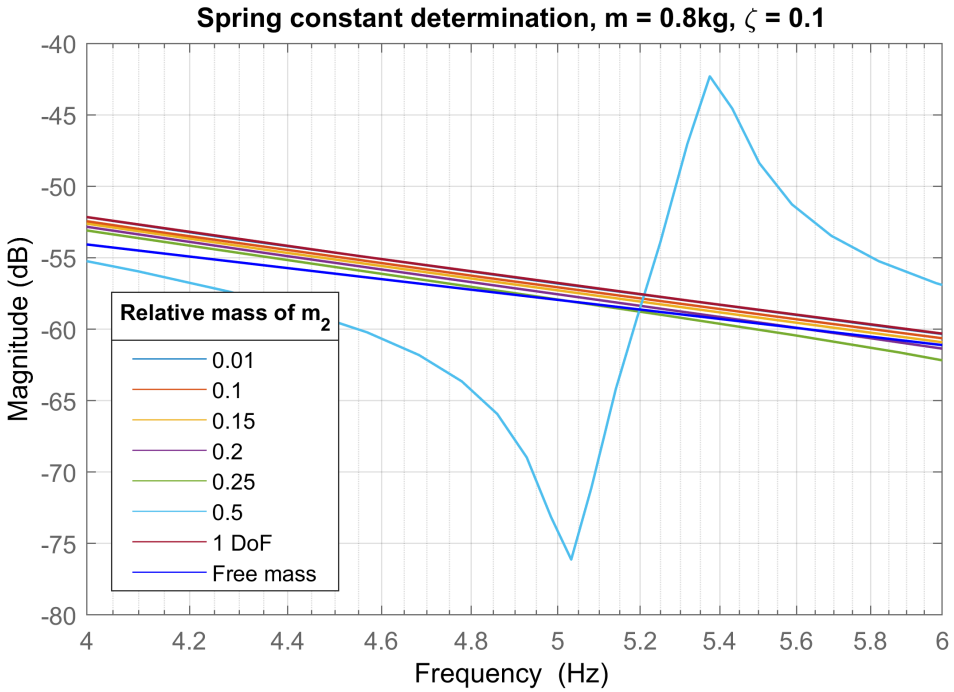

Figure 3.8: Effect of secondary mass relative to primary mass using spring constants found in chapter 4 zoomed into the range of 4-6 Hz.

In figure 3.8 we can see that having a secondary mass could even be useful as it brings the predicted response closer to the ideal, free mass, in terms of decibel difference at the cost being at

a steeper slope. On the other hand, if this secondary becomes too great the dB difference becomes larger again to the point of having resonance and anti-resonance within the operating frequencies. A secondary mass limit is set at 15% as this enables us to work with the assumption of it being negligible for ease of dimensioning with it giving a decent representation of the actual behavior.

4 Dimensioning

This chapter will employ the methods outlined in chapter 3 to determine the dimensions of the test setup. First the leaf spring dimensions will be found. Second the distance between the plates will be determined.

4.1 Leaf spring dimension determination

4.1.1 Determining k_t

To determine the dimensions of the leaf springs the total spring constant k_t must first be determined. This is done by choosing k_t such that the bode plot closely resembles that of the unhindered Robird body oscillation, which is modeled as just a mass subjected to a harmonic load. The mass of a Robird is approximately 0.8 kg (not including the top block) and operates at frequencies between 4 and 6 Hz. Using this, and an estimated damping coefficient of 0.1, the bode plots of the system with five different values of k_t are plotted in figure 4.1.

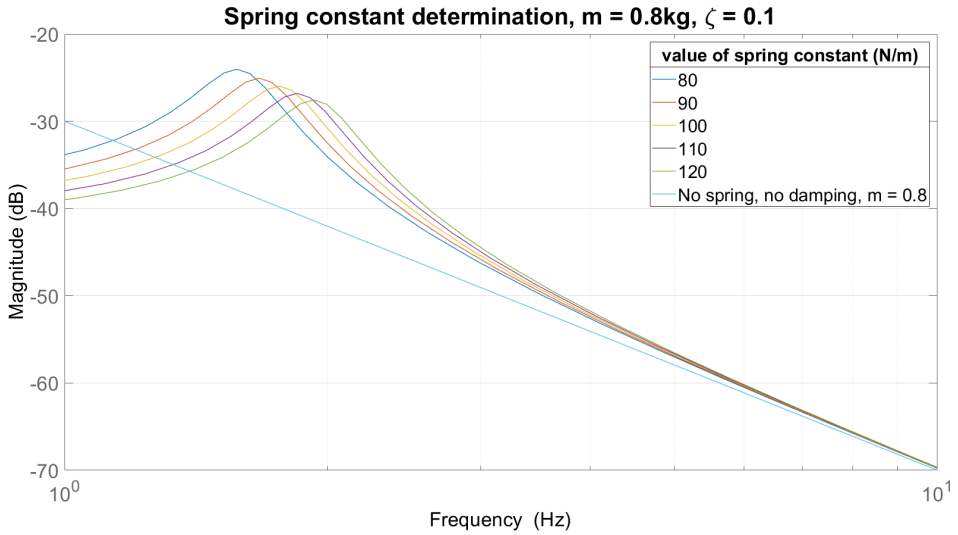

Figure 4.1: Bode plots of five values for k_t ranging linearly between 80 and 120 N/m. A reference bode plot of a 0.8 kg mass is also included.

Perhaps unsurprisingly, the lower the value of k_t the closer the system gets to the reference line between 4 and 6 Hz. However, this does not mean that k_t should simply be as small as possible. The lower k_t the more it will deflect to counteract the lift force generated by the Robird beyond that which it generates to compensate its own gravity. A low k_t to perfectly match the reference would require a spring that would have dimensions that are simply too impractical. Therefore a trade-off will have to made. As was stated in chapter 2 the maximum additional weight that the Robird can carry while still being able to generate enough life to fly is 70 g, meaning that the lift generated is roughly equal to 8.7 N. Now suppose that the additional mass is zero, leading to 8 N of weight then the springs need to be able to prove the additional 0.7 N. Therefore, it was chosen that a k_t of 100 $\mathrm{N\,m^{-1}}$ would be used, leading to at most a 0.7 mm base deflection due the generated lift. This value for k_t also gives a response within the allowed offset of 5 dB for the springs to have reasonable dimensions, as will be discussed in the next section. To ensure that at this value of k_t the system could accommodate a different mass and damping coefficient than those used in figure 4.1 sensitivities tests for those are shown in figures 4.2 and 4.3 respectively.

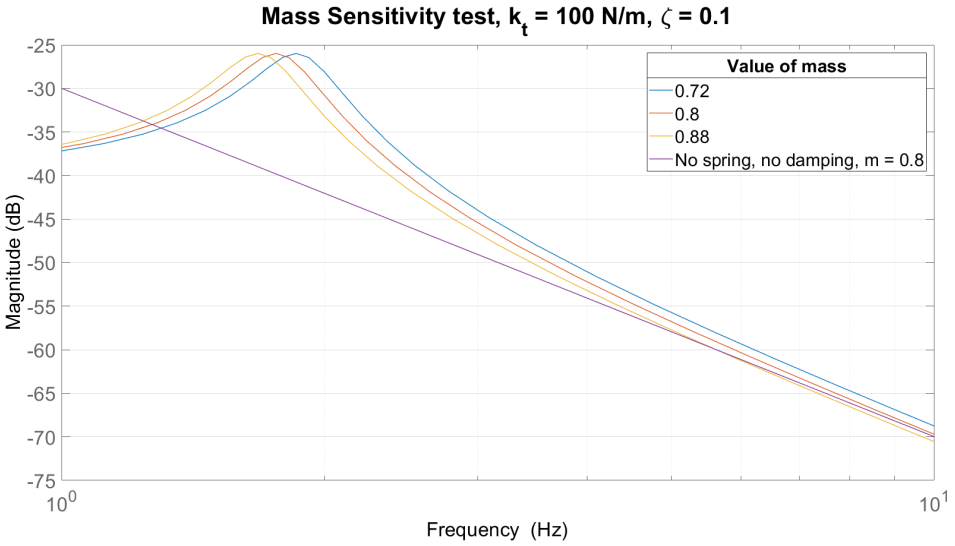

Figure 4.2: Mass sensitivity test using a 10% margin around the expected mass, thereby covering the additional mass restriction.

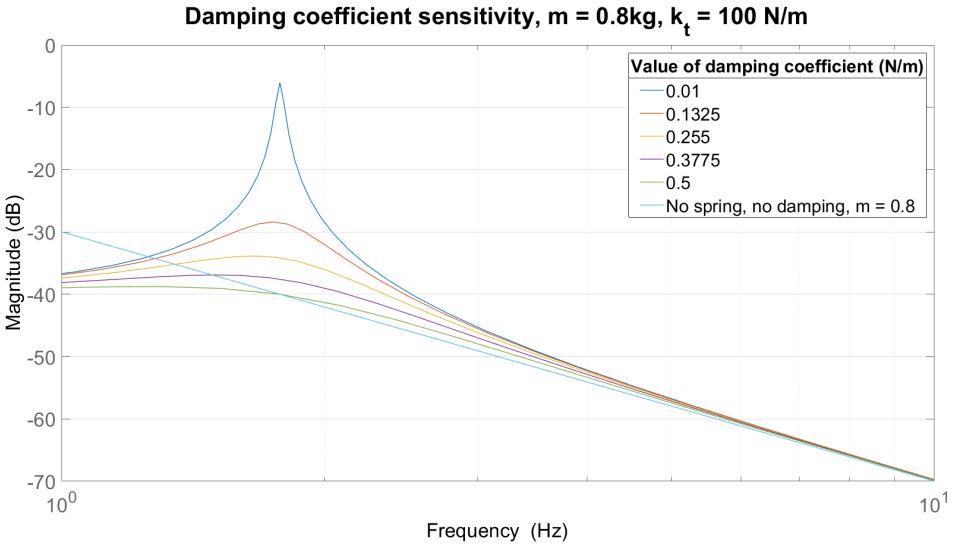

Figure 4.3: Damping coefficient sensitivity test using five damping coefficients ranging linearly between 0.01 and 0.5.

As can be seen in the sensitivity tests, while mass seems to have some effect damping has no significant effect on the response. While it would be odd for the mass of the Robird and the top block to be lower than the estimated mass for the Robird, even a 10% decrease would yield a transfer function offset that is still within the allowed range. If the total mass is heavier than the Robird then the systems appears to more accurately resemble the motion of the Robird in flight. However, how much additional weight can be added is limited but it useful to know that additional mass will not hinder the response.

The systems seems to be insensitive the mass and damping changes enough to continue with a k_t value of $100\,\mathrm{N\,m^{-1}}$ to find the dimensions of a single leaf spring plate.

4.1.2 Determining single leaf spring plate dimensions

Since $k_t = 4k_{eq}$ each set of parallel plates should have a spring constant of an k_{eq} of 25 N m^{-1}. The stainless steel that is available for use is of type 1.4310 at thickness ranging from 0.1 mm to 1 mm in 0.1 mm increments. Using equation 3.4, the now known value for k_{eq}, the known options for plate thickness, and steel's Young's modulus of 200 GPa (MakeItFrom.com, 2018), the possible combinations of b and L for each plate thickness can be plotted. This is shown in figure 4.4.

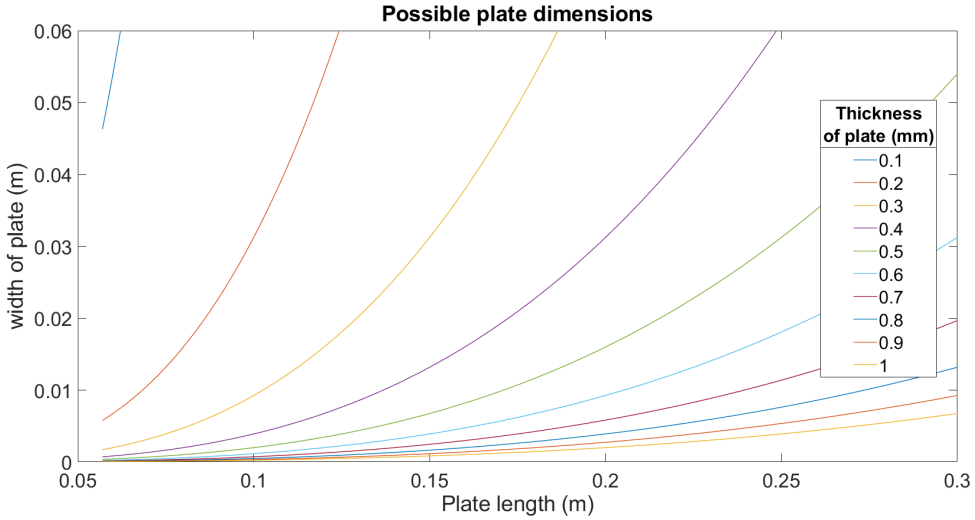

Figure 4.4: Possible dimensions of each leaf spring for the desired value of $k_t = 100$ N/m.

However, to ensure that the assumptions used in chapter 3 hold, care must be taken that the plate is long enough and doesn't receive too much stress. As stated in chapter 2 the leaf springs must still show elastic and linear behavior for a total deflection of 2.5 cm. If each set of parallel springs will deflect a total of 2.5 cm then each plate will deflect at most 1.25 cm. As this is allowed to be at most 22% of the plate length the minimum length for each plate 5.7 cm for the linear behavior assumption to hold. Furthermore, the material has a tensile yield strength between 210 and 1080 MPa and a fatigue strength between 210 and 600 MPa, this depends on further treatment of the steel which is unknown (MakeItFrom.com, 2018). To ensure there is no plastic deformation or fatiguing, it was decided that the springs should not 80% of the lowest stress value of 210 MPa. The stress plot at a deflection of 1.25 cm is shown in figure 4.5.

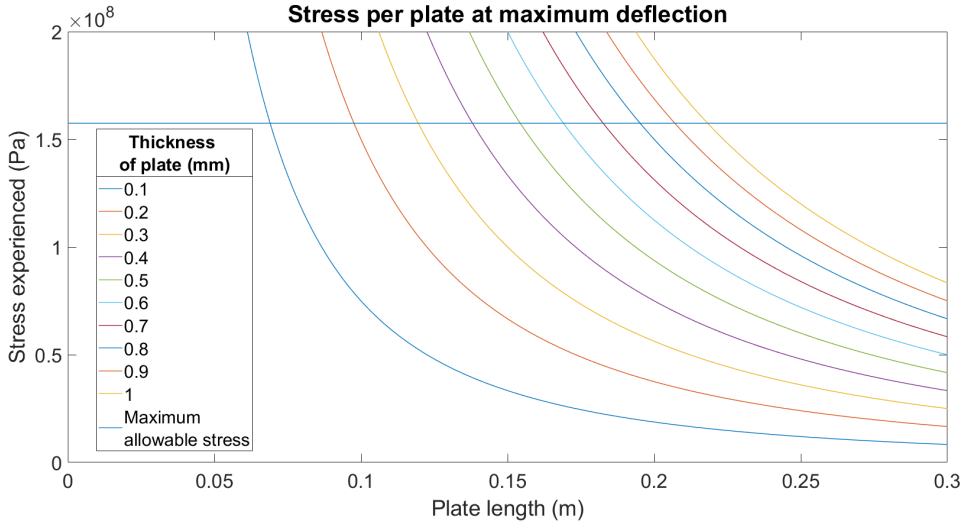

Figure 4.5: Plate stress as a function of its length at the possible thicknesses.

By combining the information in figure 4.4, figure 4.5, the minimum length of 5.7 cm, and the physical restrictions the dimensions of the plate need must be determined. It is ideal to make the springs as long as possible while still staying within the allowed restriction as this allows for greater deflections before linearity and stress limits are reached. To allow for sufficient space left for the side blocks and top blocks to be added the dimensions of the plates are chosen to be15 cm, 1.32 cm, and 0.4 mm. Using these dimensions, the steel's Young's modulus of 200 GPa and shear modulus of 77 GPa (MakeItFrom.com, 2018) it is calculated that each parallel leaf spring set has a k_{eq} and $k_{\theta eq}$ to:

$$k_{eq} = \frac{2 \times 10^{11}(0.0132)(4 \times 10^{-4})^3}{2(0.15)^3} = 25.03\,\mathrm{N\,m^{-1}} \tag{4.1}$$

$$k_{\theta eq} = \frac{7.7 \times 10^{10}(0.0132)(4 \times 10^{-4})^3}{6(0.15)} = 0.0723\,\mathrm{N\,m\,rad^{-1}} \tag{4.2}$$

4.2 Distance between front and back springs

To find the distance between the front and back springs the moment of inertia was needed but this was not initially known. To determine this both a simulation and a experimental approach to reduce the chance of mistakes. They yielded similar results of a moment of inertia of $0.0087\,\mathrm{kg\,m^2}$. Using the same approach as the previous section a bode plot of the the pitching mode at varying distances to the center of mass can be found in figure 4.6.

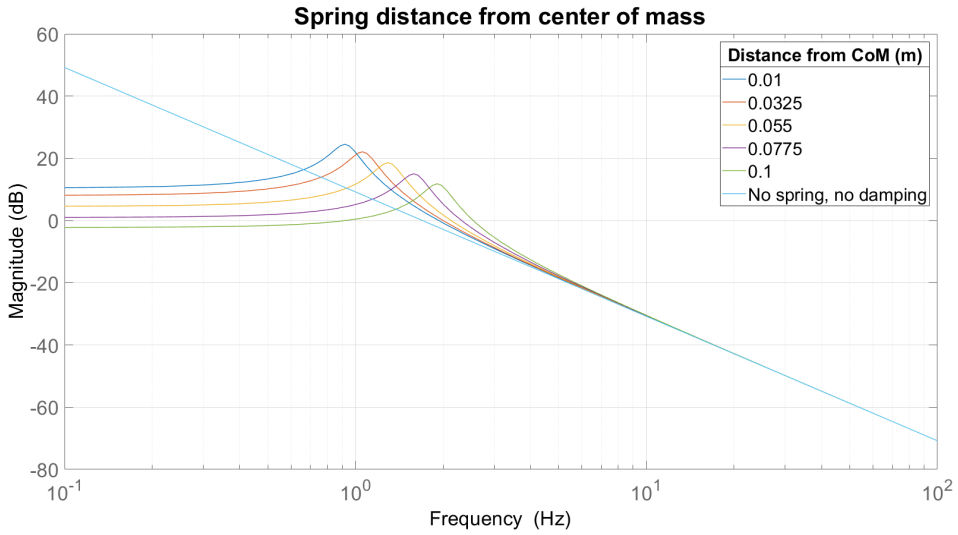

Figure 4.6: Bode plots of five values for r ranging linearly between 0.01 and 0.05 m. A reference bode plot of a 0.0087 kgm^2 is also included.

It was decided to go for a distance to the center of mass from the plate center of 3 cm, so a 6 cm distance between the plates. This seemed to be the best distance where it is possible to mount the Robird on top of the top block and have a good transfer in the operating frequencies.

5 Design

This chapter will discuss the details of the design of the test setup and consists of two main parts. First, the design of the side and top blocks and the leaf springs. Second, the sensors to be used for measuring the top block's displacement.

5.1 Block design

While the material of the leaf springs was already known to be stainless steel 1.4310, the material of the top and side blocks is still left undetermined. The material would have to be lightweight, readily available, and able to be made with precision. These factors left two main contenders: connected laser cut delrin plastic plates or 3D-printed plastic. Laser cutting had the advantage of being more accurate, being able to cut accurately to a tenth of a millimeter, and delrin being a stiffer material than what could printed, but had the disadvantage of only being able to fully cut through plates in one dimension. This would mean that individual plates would need to be designed and slotted into each other, which imposes additional design restrictions. It was decided that the advantages outweighed the disadvantages so the blocks would be made of laser cut delrin plates.

The top and side blocks were designed in such a that the length of the leaf springs and their distance from the center could be adjusted. This was done in the case that the predicted response described in chapter 4 was shown to be inaccurate. This does also mean that it might be necessary for the blocks to be larger and heavier than would be ideal.

It should also be noted that two versions of the side and top blocks were made, one a lighter version than the other. When the first version designs were realized it was decided to move onto testing with those while the new version was made. This would also give insight into the effect of the mass of the side block. However, both these versions will be displayed here one after the other.

5.1.1 Side block

First version

When beginning on the design of the side blocks it was desired to find a way through which the length of the leaf spring could be easily changed without any other changes to its properties and not allowing it to shift in the y-direction once the length is set. This consideration should not weaken the main purpose of the side blocks to allow for distance between the top and bottom block for distance measurement and the leaf springs should still be properly clamped.

Clamping the leaf spring could be done best by placing it in between two delrin plates and keeping these together with nuts and bolts. This way tightest possible clamp could be ensured by screwing the bolts as tightly as possible. It is not reliant on everything fitting together perfectly such as through a connecting plate and it does not wear away through use quickly as opposed to using glue.

Two sets of these clamping plates are connected on either side of two walls, the length of which determines the height of the top block. It was decided to use a length of 6 cm, this was done to allow enough for the top block to oscillate while leaving enough distance for any potential distance sensor to be in their effective range.

Making the length adjustable was done by creating small groves of 0.4 mm depth in these two walls that the leaf spring can slot into, preventing shifting. It would also have been possible to make a series of holes in the clamping plates, one in the leaf spring, and use a nut and bolt to

keep in place. However, this would result in a greater mass of both the clamping plates in the second version due to the support required for the holes.

Figure 5.1 shows the first version of a side block, which has a mass of 32 g. The leaf spring's length can be varied between 13 cm and 16.5 cm in steps of 0.5 cm

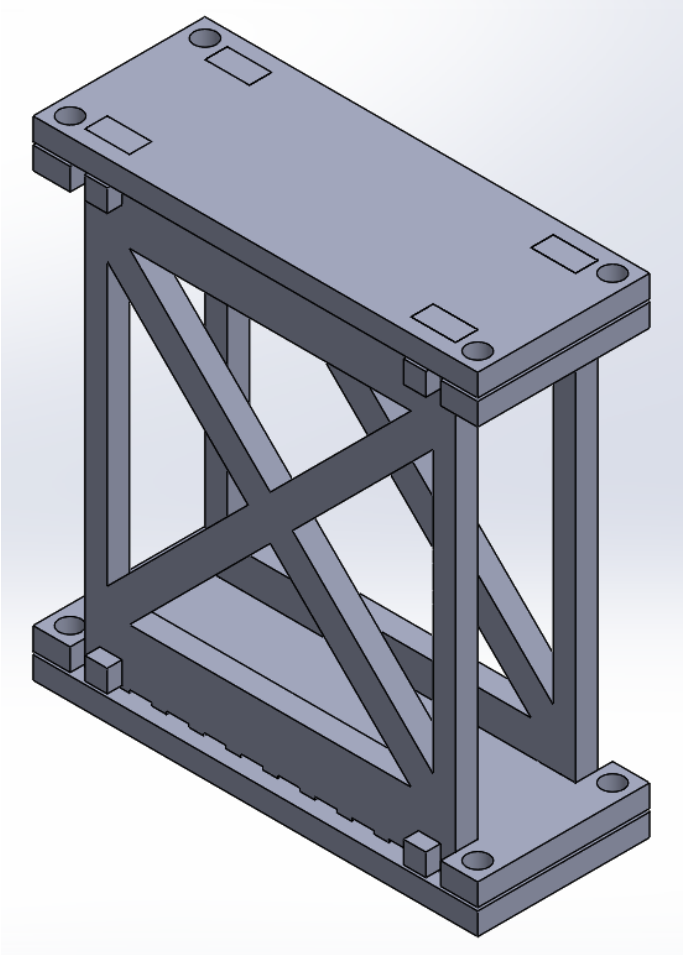

Figure 5.1: First version of the side block. Two clamping plates are at the top and bottom. The lower clamping plate slides into the side walls and the upper is fitted on top. The groves where the leaf spring slide into can be seen at the bottom. The total dimensions are 2.32 cm by 6 cm by 6.6 cm in the x-, y-, and z-direction respectively.

5.1.2 Top block

First version

Seeing as the side blocks will allow for the leaf springs to be adjustable in length this is not necessary for the top blocks. Instead, the top block will allow for the distance to the center to be adjusted.

In similar fashion as before, the leaf springs will be secured by clamping them in between two plates. However, this time the nuts and bolts will go through the leaf springs to completely fix it to the plates. By making more holes farther and closer to the center of the plate the distance to the center can be adjusted. These two plates are connected to two walls which also connect to the top plate. For this top block it was of interest for the top block to be easy to disassemble for testing purposes. This is why the choice was made to make of an L-bend locking mechanism, which is pushed through a slot and then shifted to lock it in place. The height of the top block was chosen such that the wings would high enough that they would not hit the side blocks.

Figure 5.2 shows the first version of the top blocks, which has a mass of 55 grams. The distance of the leaf springs to the center can be either 3.5, 3, or 2.5 cm.

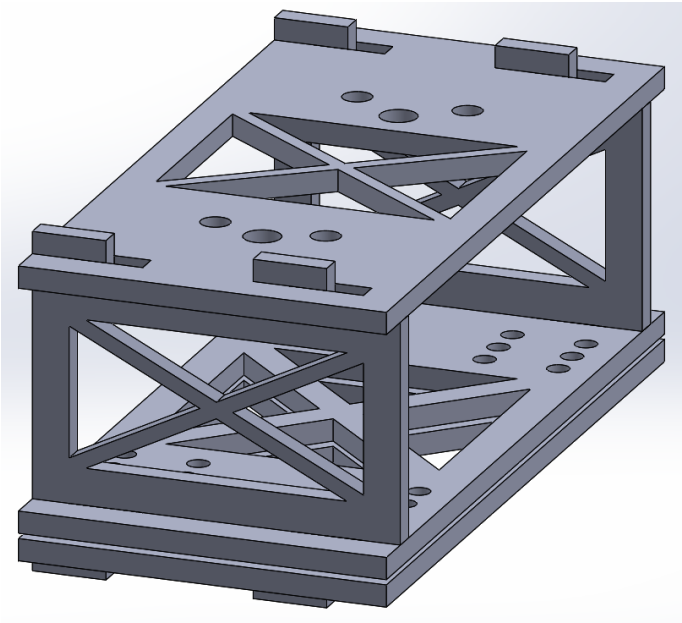

Figure 5.2: First version of the top block. The side walls are fitted with the L-bends which the other plates are slotted into and then shifted to the right. The total dimensions are 10 cm by 5 cm by 4.54 cm in the x-, y-, and z-direction respectively.

5.1.3 Leaf spring

Two leaf springs are shown in figure 5.3, with a total mass of 18 grams.

Figure 5.3: The leaf springs that will be used. The protrusions at the ends fit into the groves of the side block and the holes in between the two clamping plates of the top block. The total dimensions are 1.92 cm by 47 cm by 0.4 mm in the x-, y-, and z-direction respectively.

Instead of having eight separate leaf springs it was thought to be more practical to make one sheet metal cut out that would span across the setup. This would also cause a better clamping of the springs at the top block.

5.1.4 Second version

The reduce the mass of the side and top blocks the thickness of the plates was reduced to 2 mm from 3 mm and the solid sections had shapes cut out of them which best suited the available area. The decision was made to not simply cut solid sections out entirely as this would lead to too great a loss in structural integrity, and would reduce the effectiveness of the leaf spring clamp to too great an extent.

Figure 5.4 shows the second versions of the side and top blocks, which have a mass of 14 g and 32 g respectively.

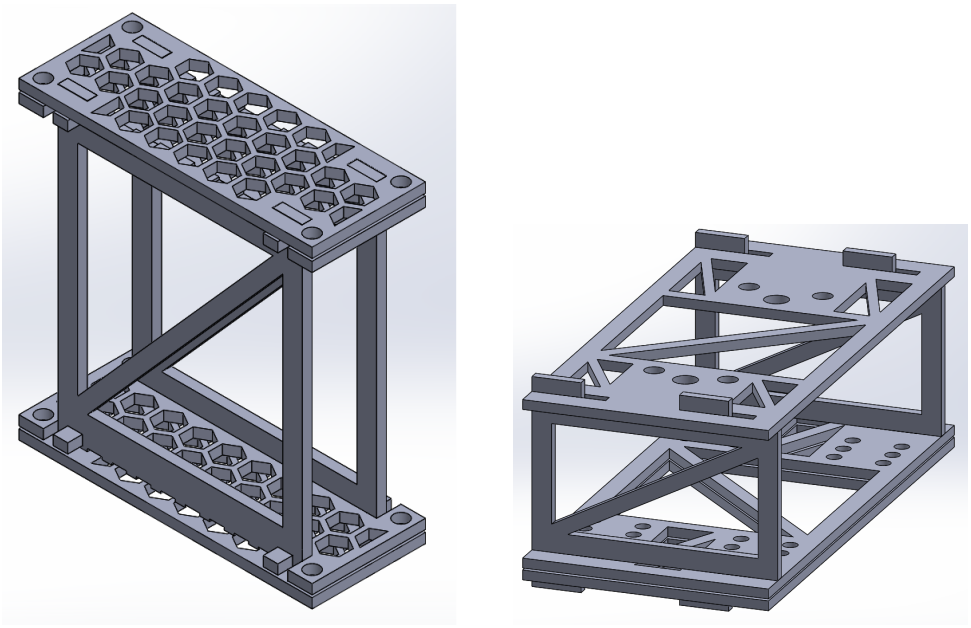

(a) Second version of the side block. **(b)** Second version of the top block.

Figure 5.4: Second version of the two blocks. For the side block hexagons were cut out of the clamping plates to allow for greater mass reduction. The dimensions of the new side block are 2.32 cm by 6 cm by 6.42 cm in the x-, y-, and z-direction respectively. The dimensions of the new top block are 10 cm by 5 cm by 4.24 cm in the x-, y-, and z-direction respectively.

5.2 Sensor investigation

During a test in a wind tunnel it needs to be possible to measure the displacement of the top block continuously without affecting its motion. This also needs to be done at two different locations along the length of the Robird. In order to have no effect on the motion a non-contact method of sensing is required. This leaves two options for measuring the distance: ultrasound and light based sensors.

Both of these sensors operate by sending some kind of wave measuring and the time it takes for it to return to the receiver. Since the speed of the wave is known the distance it has traveled can be calculated. There are two significant differences between these two sensor types: effective range and cost.

Light based 'Time-of Flight' sensors (ToF) can vary greatly in the minimum distance the object needs to be away from the ToF sensor. For example, the VL53L0 can measure between 50mm and 1200mm ADAFRUIT WEBSITE SOURCE, the VL6180x between 5mm and 100 mm (sometimes 200 mm with good ambient conditions) ADAFRUIT WEBSITE SOURCE, and the RFD77402 can measure between 100 mm and 2000 mm SPARKFUN WEBSITE SOURCE. In contrast, ultrasound sensors have a consistent minimum with both the HC-SR04, HC-SR05, and US-020 having ranges of 20mm-4000mm, 20mm-4500mm, and 20mm - 7000mm, respectively.

Ultrasound sensors are typically significantly cheaper as compared to light-based sensors. Typical costs for a low-cost ultrasound sensor range between roughly €2.5 to €6 as compared to roughly €13 to €30 for ToF sensors.

Bases on these considerations it was decided to use two Adafruit VL6180x ToF sensor due to their short minimum distance and relatively low cost as compared to other ToF sensors. This does mean that the height of the side blocks can be lower, but this could not be implemented due to lack of time.

5.2.1 Sensor implementation

The Adafruit VL6180X ToF sensors are to be implemented using an Arduino UNO microcontroller. The sensors were revealed to have one complication: they communicate through the I^2C protocol but the two sensors have the same address which cannot be changed (Adafruit, 2018). Therefore, something will have to be done to allow both sensors to operate on the same I^2C bus.

First, it was attempted to connect the sensors' V_{in} pin to separate digital pins on the Arduino, allowing them to be turned on and off by changing the pin setting. Then a sensor can be turned on, the distance read, and turned off before turning the other sensor on and doing the same. When implemented this worked well for a time but eventually one of the senors would freeze during the distance read. Which sensor was affected varied but it seemed to occur after roughly the same amount of time. It was also noticed that this would only occur if V_{in} was being periodically switched between high and low.

The same principle could be attempted using the sensors' shutdown pin, which could result in better operation, but could also yield the same result. Instead, it was decided to use a multiplexer, which enables devices with the same address to be connected to the same I^2C simultaneously.

6 Testing

This chapter will discuss the validation of the constructed design. First, the test method for the test setup will be explained, followed by the results with a comparison to the expected response as derived in chapter 3.

6.1 Test method

In order to determine the transfer function of the test setup a modal hammer will be used in combination with accelerometers, connected to channels one and two. A modal hammer operates by applying an impulse to the setup and using the accelerometers to measure the response. In theory a perfect impulse contains all frequencies but in practice it is simply a very large range of frequencies. The modal hammer uses software that determines the accelerometers response for every contained frequency and compares it with the input it gave. It then takes the ratio between these two to determine the transfer function.

To approximate a realistic response of the Robird, a test mass was made. This consisted of a carbon rod with identical discs of lead attached to it on either side of the center. The total mass was of the setup was set to be 0.8 kg and the distance of the discs to the center was determined such that it would have the same pitching moment of inertia as the Robird. By attaching this to the top block the motion of the Robird may be approximated. The entire setup was placed on its side to neglect the effect of gravity. The test mass is suspended using a 0.54 m string such that the entire test setup is of an equal height.

By hitting the test mass in the centre with the modal hammer the oscillation response can be determined. By hitting the at the top or bottom, the pitching response should become apparent by contrasting it with the oscillation response.

6.2 Results

In this chapter example trials will be used for the purpose of showcasing the response and analyzing the response. Other trials can be found in Appendix B. Discussion of the quality of the sensors themselves can be found in chapter 7

As the testing method creates a transfer of acceleration against force applied the transfer functions shown in chapter 3 must be differentiated twice to compare properly. This is done by simply multiplying the transfer functions in chapter 3 by s^2.

During testing a general observation was made that the accelerometers the testing method had difficulty in determining the transfer function below 1 Hz, with results being being very inconsistent. It was also noticed that seemingly at random the channel 2 sensor would show a transfer which began at a magnitude around 50 Hz and would gradually decrease. The channel 2 sensor would also exhibit two other distinct consistent peaks around 3 Hz and 5 Hz regardless of being placed at the top or bottom of the top block. These effect are seen as sensor errors and will be neglected during the results analysis.

6.2.1 Oscillation

Version 1

The response of version 1 of the test setup can be seen in figure 6.1. The predicted response was made using equation 3.10 (multiplied by s^2). The spring constant k, as identified in figure 3.6, for the predicted response was calculated using 3.5 multiplied by four. The masses m_1 and m_2, also identified in figure 3.6, were determined as followed:

$$m_1 = m_{bird} + m_{tb} + m_{lf} = 0.8517\,\text{kg} \tag{6.1}$$
$$m_2 = 4m_{sb} + 2m_{lf} = 0.0899\,\text{kg} \tag{6.2}$$

Where m_{bird} is the mass of the Robird, m_{tb} the mass of the top block, $m_{[}lf]$ the mass of the leaf spring, and m_{sb} the mass of the side block. As the total mass of the steel plates is 18 g it should be considered when determining the two masses in the system. This was done by adding half of a leaf spring's mass to either m_1 or m_2 for each leaf spring connected to it. For example, each side block has two leaf springs attached so the mass of one leaf spring is added to each side block. The other halves of the leaf springs mass go the bottom block which is fixed and the top block. Then because there are four side blocks, m_2 is found by summing these. This approximation relies of the assumption that all the side blocks move in the same way.

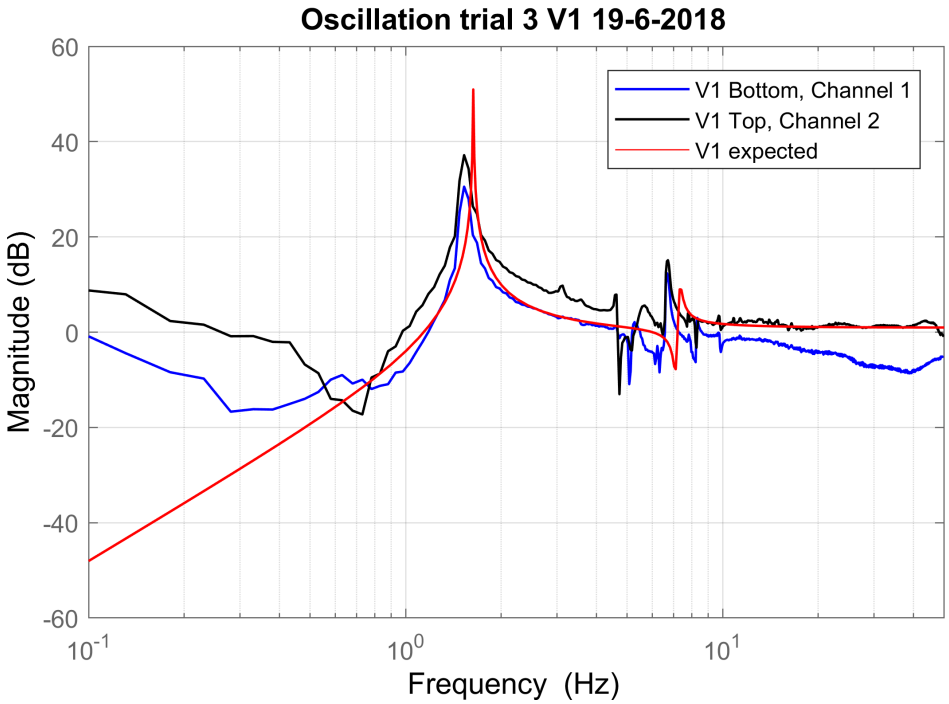

Figure 6.1: Oscillation response of version 1 of the test setup and the predicted response based on chapter 3. The expected spring constant and the measured masses were used for the predicted response

Figure 6.1 shows two clear resonance peaks: one at a frequency of 1.52 Hz and a second at 6.72 Hz. The expected response has the first peak at 1.64 Hz and the second at 7.32 Hz. These values are 8% and 9% greater than measured for the first and second peak respectively. The general shape of the model consistently matches that of the data, particularly channel 1, which suggests that the model does accurately portray reality and that this discrepancy is likely due to error in the parameters.

To check that this second peak is indeed due to the effect of the side blocks. The accelerometers were placed on those and another test was done, the results of which can be found in figure 6.2.

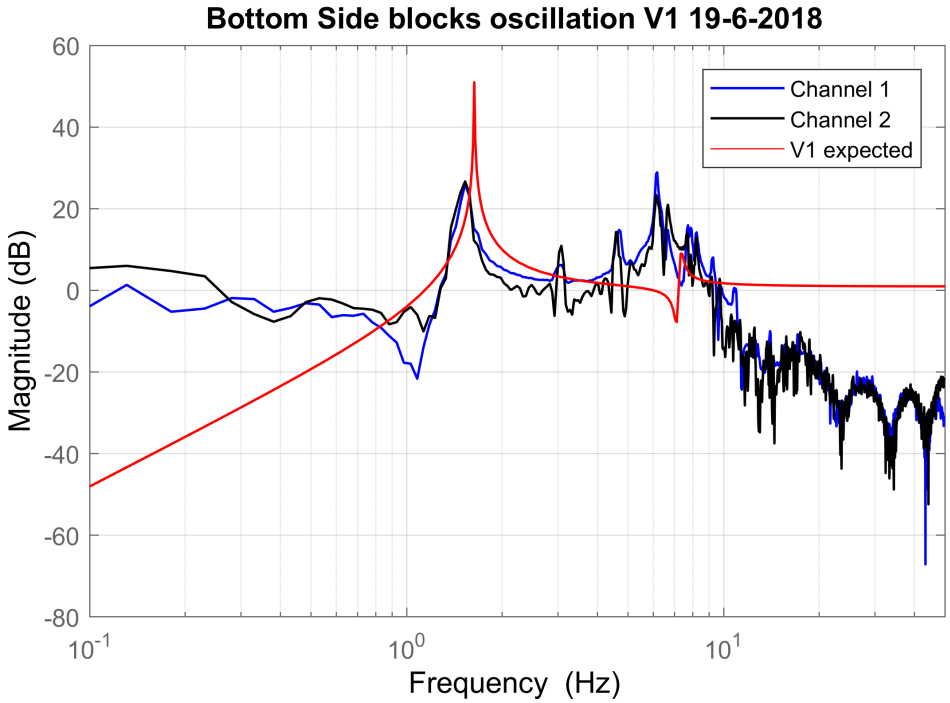

Figure 6.2: Oscillation response of the the side blocks of version 1 of the test setup while impulses were delivered to the top block. The accelerometers were placed on the lower two side blocks in this case.

As can be seen in figure 6.2 the second peak is indeed due to the effect of the mass of the side block. The resonance peak is at a lower frequency than in figure 6.1 and other resonances seem to exist close to the greatest one. This is thought be due the additional mass of the accelerometers added to just two of the side blocks.

Version 2

The results of testing the the second version of the test setup can be seen in figure 6.3. The expected response was created in the same was for the version 1 but with new values of the top and side block mass.

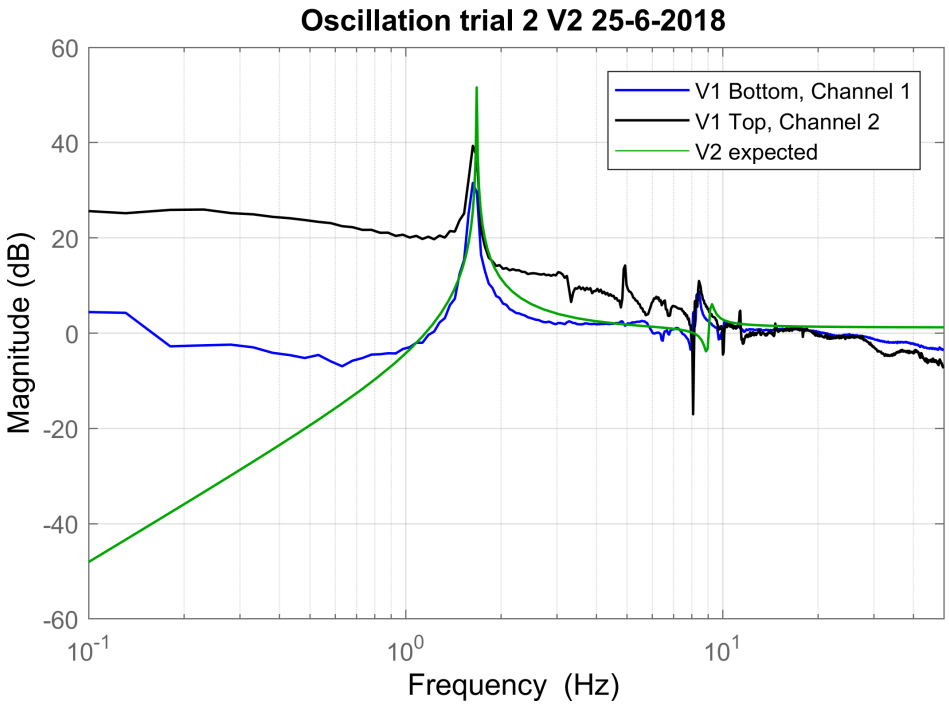

Figure 6.3: Oscillation response of version 2 of the test setup and the predicted response based on chapter 3. The expected spring constant and the measured masses were used for the predicted response

The measured response shows two clear resonances at 1.63 Hz and 8.42 Hz. The expected response shows resonance peaks at 1.68 Hz and 9.26 Hz. The predicted values are 3% and 10% greater for the fist and second peak, respectively. Once again, channel 1 seems to match the predicted response well, especially before the first resonance, and it can be said that the general model is correct. This suggests that the difference between the actual and predicted response is due to the mass estimation. To confirm this another experiment was done with the shorter springs. The result can be found in figure 6.4

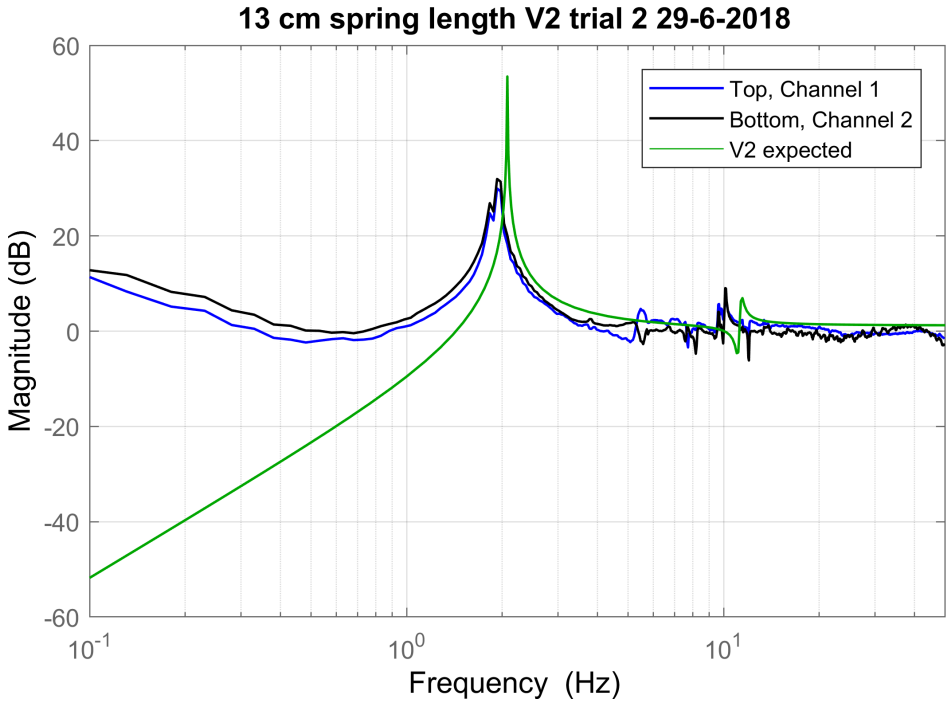

Figure 6.4: Oscillation response of version 2 of the test setup and the predicted response based on chapter 3 with spring lengths of 13 cm. The expected spring constant and the measured masses were used for the predicted response

Close to resonance the test with 13 cm follows the same shape as the predicted response but shifted to the left. This could be due to an error in the mass approximation. At lower frequencies the measured transfer differs more and more but this could also be due to the measurement error at lower frequencies. The first and second resonances occur at 1.93 Hz and 10.12 Hz, and 2.08 Hz and 11.50 Hz for the measured and predited responses, respectively. The predicted response is now 8% and 14% greater for the first and second peak respectively. With this information it is not possible to definitively state whether the spring constant is accurately modeled.

Comparison

The transfer of channel 1 of both the first and second version can be found in figure 6.5. This shows very clearly that the error is consistent with the difference between the predicted and measured responses for the second peak for version 2 being only 0.1 Hz greater than that of version 1.

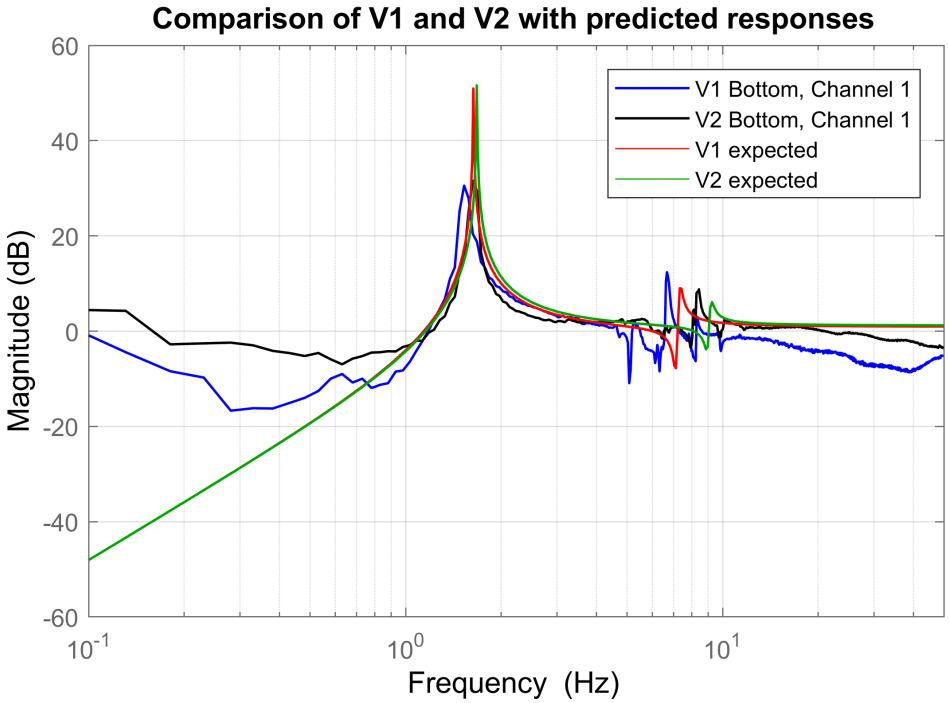

Figure 6.5: Comparison of the responses of version 1 and version 2 with both predicted responses.

6.2.2 Pitching

The pitching measurement taken for both versions of the setup were inconclusive, showing only a noisier shape of the oscillation behavior. This could be due to the measurement error up to around 1 Hz, which is where we expect the pitching system to resonate. This can also be due to other errors discussed in chapter 7.

7 Discussion

In this chapter the entire assignment will be evaluated. Problems in every phase of the report will be identified, its effect explained, and possible improvement suggested. First problems and their effect will be identified by chapter, followed by possible improvements to the test setup to alleviate these.

7.1 Problems

Requirements

The second version of the setup fulfills the requirements fairly well. It is fixed in the x-direction but not entirely in the y-direction. If all side blocks experience a force in the y-direction then the lower leaf springs will have to bend to counteract this. This would only happen if the Robird would apply a force to all side blocks in the same direction. While this is highly unlikely, it isn't entirely fixed. The setup does allow for oscillation in the z-direction, pitch, roll, while keeping yaw fixed. The system also stays within the 5 dB offset, with the maximal theoretical offset being 0.7 dB and the measured offset at most 1.9 dB, which includes possible signal noise and other errors. The setup also allows for at least 2.5 cm of deflection in the z-direction. Each spring can deflect about 1.85 cm before it is at 95% of both its fatigue and yield strength leading to a maximum deflection of 3.7 cm. The setup measures 10 cm, 49 cm, and 15 cm in the x-, y-, and z- directions respectively, so it is within the spatial requirements. The additional mass added to the Robird is m_1 described in chapter 6 without the Robird's mass, giving a total of 47.7 g which is well within the allowed additional mass. The measurement method is working but currently the ToF sensors don't fit on the setup and the data can't be stored yet.

So the test setup meet all but two requirements. Namely, it is not entire fixed in the y-direction and the sensors cannot yet be implemented.

Mathematical Analysis

The model models the behavior of the system well and the systems operates within the boundaries where the assumptions made are valid. It could be worthwhile to determine a model for the pitching behavior which includes the secondary masses. It is not known how k_θ changes with deflection.

Dimensioning

The dimensioning procedure went well and since the model works well no major problems are identified in this chapter.

Design

The side blocks are larger than they could be to allow for leaf spring length changes to be made easily. When the setup was built the side blocks, the top block, and the springs, were heavy enough to already cause a significant deflection of the bottom leaf springs due to gravity. This constant offset severely reduces the operational range of the Robird.

The L-bend mechanisms used to keep the top block together relies on static friction to stay in place. During testing there were no problems with this design but the roll of the Robird might cause these to shift loose.

Since the displacement sensors were chosen after the blocks were designed it is unfortunate that they cannot be easily incorporated into the design as of yet. What is more important however is that the Arduino currently can't function without a laptop and there is no way to store

the displacement data automatically. The ToF sensors also need to be tested to determine any potential permanent offset, error margin and minimum reliable distance.

Testing

Oscillation measurement went very well except for an error in parameter estimation. The spring constant could be different than expected due to small changes in the thickness of the leaf spring. Since the spring constant is related to the cube of the thickness, and its already very thin in at 4×10^{-4} m. When the leaf springs were laser cut small burrs were seen on the edges of the metal. While these were filed away small remnants could leave the surfaces of the leaf spring quite rough relative to its thickness. For the mass estimation the approximation that the distributed load of the leaf springs is split equally might not be entirely accurate either. However, the initial peaks of the measurements and the prediction were always close together indicating that the error is not too great. The second resonance peak is very sensitive with respect to the size of second mass as can be seen in figure 3.7.

The pitching measurements yielded no useful results. This could be due to effects from the side blocks that have not been considered, but it is also hindered by measurement errors and the testing method. The accelerometers gave very inconsistent results around 1 Hz and lower, making it difficult to find the resonance peak of the pitching. The channel 2 accelerometer also appeared to be faulty, showing additional measurements peaks regardless of placement and occasionally producing entirely unrealistic data.

It is also likely that due to the strings that were used to keep test mass in the air the pitching behavior was severely hindered. If the test mass pitches these strings would also apply a reaction force, keeping it upright. This was qualitatively tested by pitching the free hanging mass, and it would barely oscillate when released at a small angle. The moment of inertia of the test mass was also not checked after it was made.

7.2 Improvements

7.2.1 The actual setup

The most critical improvement that needs to be made is to reduce the additional mass. The easiest way to this is redesigning the side blocks. They can be made shorter the functionality of the length adjustment can be removed, discarding a significant amount of material. Figure 7.1 shows a possible new version of the side block which has a mass of just 3.57 g, just 23% of the second version of the side block.

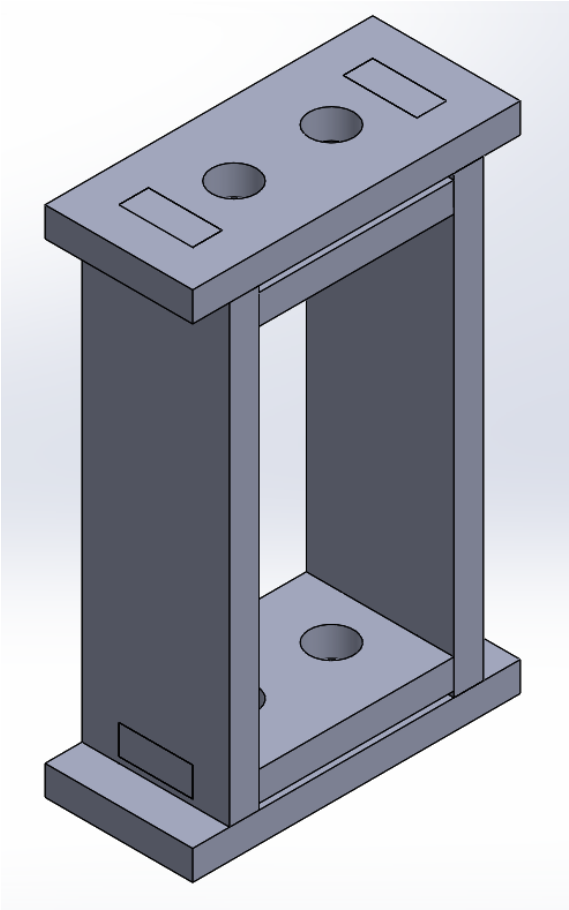

Figure 7.1: Proposed third version of the side block, which sacrifices spring length adjustment for reduced size and weight. The total dimensions are: 2.22 cm by 1 cm, by 3.48 cm in the x-, y-, and z-direction respectively.

For the top and bottom block a more rigid connection than the L-bend can be made by connecting the plates in a manner similar to the side blocks.

It is possible to power an Arduino using an external battery, and to store data on an SD-card which comes with other breakout modules. It would be ideal if it were also possible to activate the measuring from a distance, that the user can wait with measuring until the Robird has brought itself up to the leaf springs neutral position. Space for the ToF on the top of the bottom can be made by making it just 0.5 cm broader, staying within the physical limits, and holes would have to be made to allow the pins to go through. The Arduino already fits inside the bottom block, but it would have to be made longer to also allow an SD-card breakout to fit. This should be doable with the 10 cm left.

The bottom block needs to adjusted to allow for the ToF sensors to be placed in them. It would be best if there was room underneath for the Arduino, a battery to power it, and the SD card to save the data on.

To fix motion in the y-direction a wall for the side blocks could be used. Then they can then move freely up and down but when they move too far in the y-direction they are stopped.

If it is desired to use the test setup outside of a wind tunnel then an extension could be designed. For example, a weak spring with a large preload is used to suspend the Robird in the air.

7.2.2 Testing method

A simple test that should be done is placing known weights on the top block and determining the spring constant experimentally. This planned for initially but was neglected to focus on the dynamic behavior of the system and the ToF sensors, since the oscillation response was quite close already.

One test that needs to done is to actually place the setup in a wind-tunnel to see if it works as expected. This is critical because if the Robird cannot generate enough lift, or the setup affects the airflow too drastically this has significant implications for the design.

No conclusions could be made regarding the pitching motion of the Robird with the current testing method. A way to do this could be to make a new test where a rotational motor is used to apply a small periodic torque and the ToF sensors are used to read out the distance. This way a transfer function can be produced at the frequencies below what the accelerometers can measure, and the effect of the oscillation has been removed.

A similar test can be run for the oscillation to determine its behavior at low frequencies which can be used to estimate the accuracy of the spring constant.

For the testing method that is already in use it recommended that the accelerometers are tested beforehand to ensure that they operate consistently.

8 Conclusion

In conclusion a test setup was constructed for the Robird for use in a wind tunnel using four sets parallel leaf springs. The goal of the setup was to be able to measure the body's oscillation amplitude and pitch while it was kept in place by the setup. This was to be done in such a way that it had as little effect on the Robird's natural motion as possible.

This was done by first setting the requirements the setup had to fulfill and creating a rough sketch of the setup. Second, a mathematical model of the setup was made, taking into account the validity range of assumptions made. Third, based on the mathematical model the dimensions of the leaf springs were determined and how far apart these must be. Fourth, CAD drawings of the rigid bodies were made and the displacement sensors were chosen and programmed. Fifth, tests were done to validate the constructed setup using a modal hammer to determine its transfer function. Finally, the entire process was evaluated and improvements to the current design and testing, and new tests, were suggested.

The design functioned as expected during testing, but for actual application some masses are too great and must be reduced. A method to do this is proposed. The mathematical model simulates the physical behavior well and matches the oscillation behavior closely, albeit not perfectly due to incorrectly approximated parameters. However, work must still be done on determining the pitching behavior, the validity of that model, and the installment of the sensors on the setup and that the microcontroller can function and save data in a standalone manner. The requirements and whether the setup met them is summarized in table 8.1

Subject	**Requirement**	**Requirement met**
x- and y-direction	Fixed	x-direction is fixed, y- direction not entirely
z-direction	Oscillation within boundaries	Requirement met
θ- and Φ-rotation (pitch and roll)	Possible	Requirement met
ψ-rotation (yaw)	Fixed	Requirement met
Behavior within operating frequencies of 4-6 Hz	Max 5 dB offset from free mass oscillation and pitch	Requirement met
Minimum possible body displacement in z	2.5 cm	Requirement met
Maximum dimensions	0.2m×0.5m×0.2m (x,y,z)	Requirement met
Maximum additional mass added to Robird	70g	Requirement met
Measurements	displacement in z-direction at two points along x-axis	Sensors operational, not implemented

Table 8.1: Requirements for the test setup and whether these were achieved

Further research and design improvement can still be done by studying and minimizing the effect the test setup has on airflow around it. The roll behavior of the Robird has not been studied in this report and can still be optimized. Another direction for further investigation is studying different leaf spring shapes and bending modes for one which allows doesn't require two leaf springs to be in parallel and removing the effect of the secondary mass.

A Appendix: Final versions of individual plates

A.1 Side block

Bottom clamping plate

Thickness: 2 mm

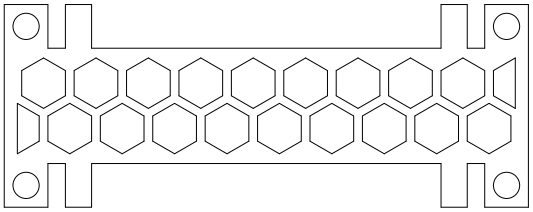

Top clamping plate

Thickness: 2 mm

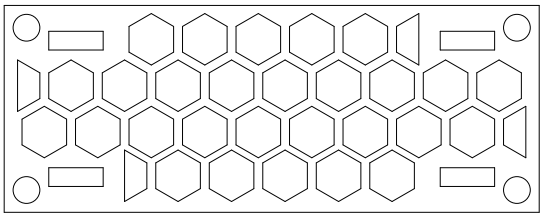

Side wall

Thickness: 2 mm

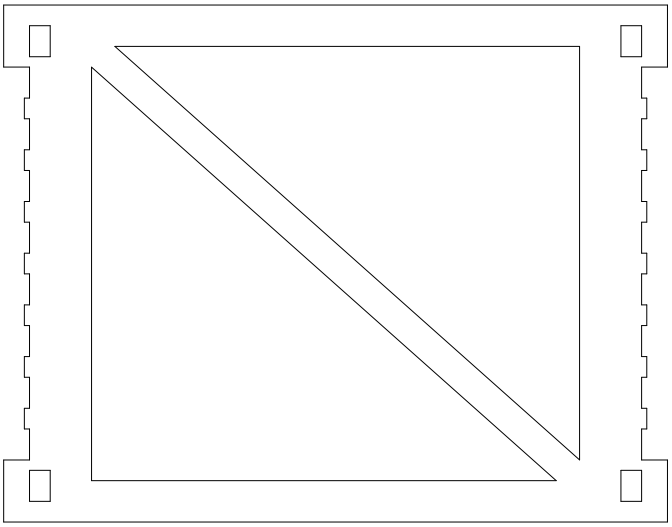

A.2 Top Block

Clamping plate

Thickness: 2 mm

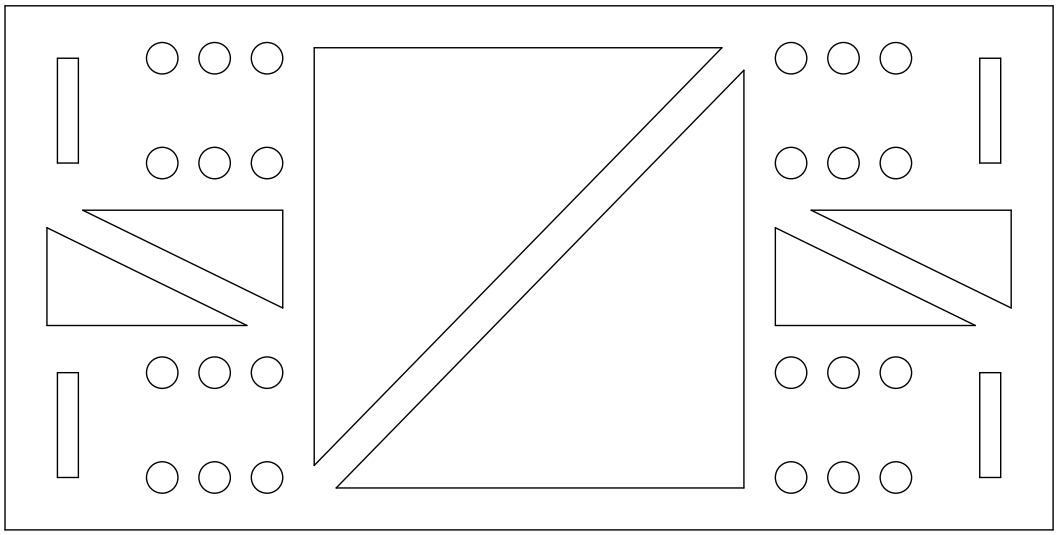

Side wall

Thickness: 2 mm

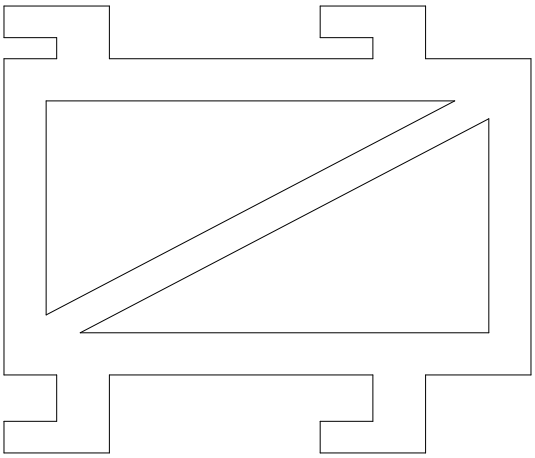

Top plate

Thickness: 2 mm

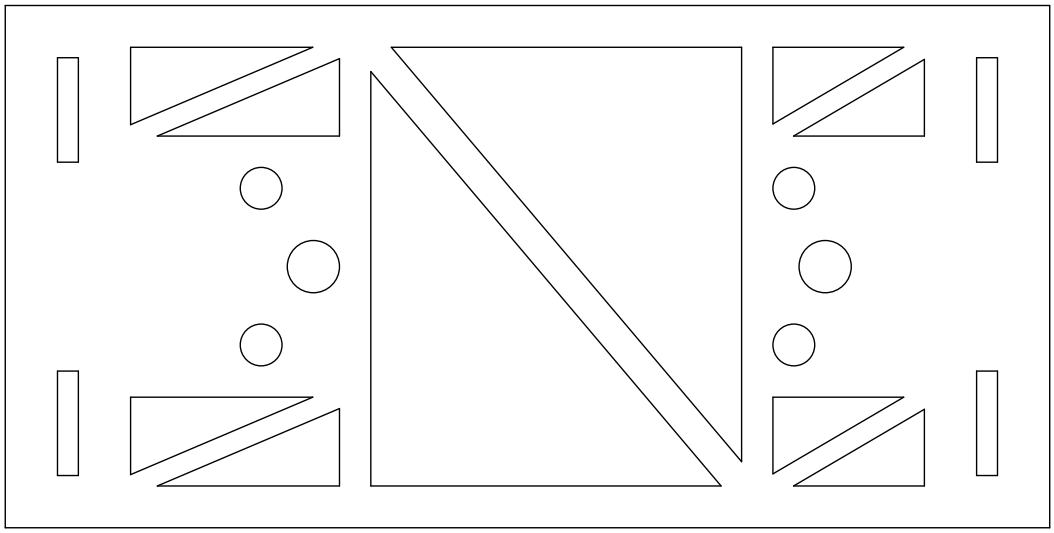

B Appendix: Other data gathered

B.1 Oscillation

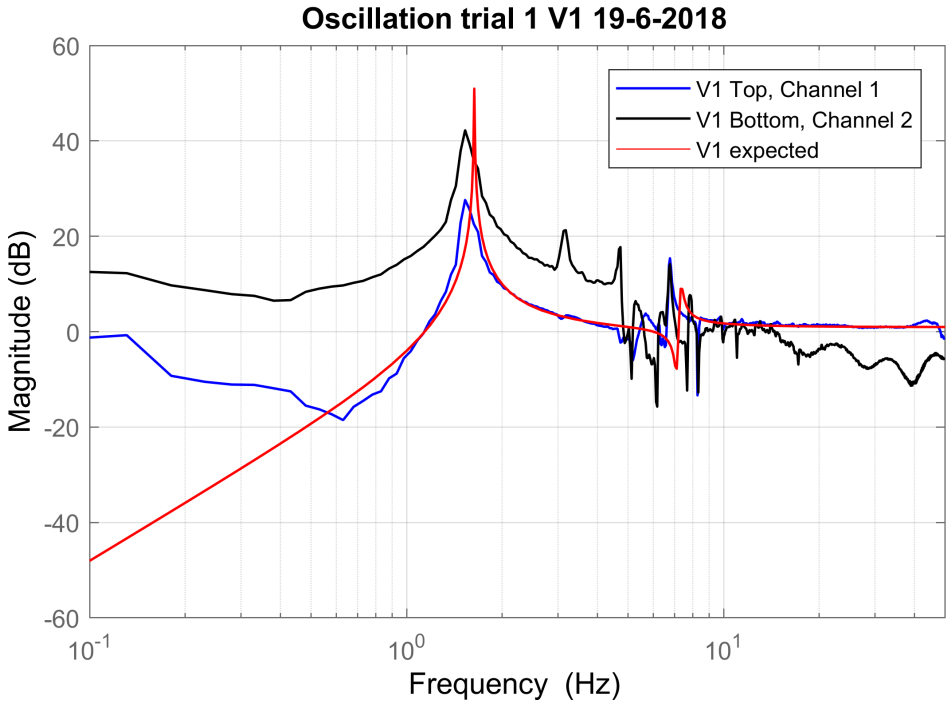

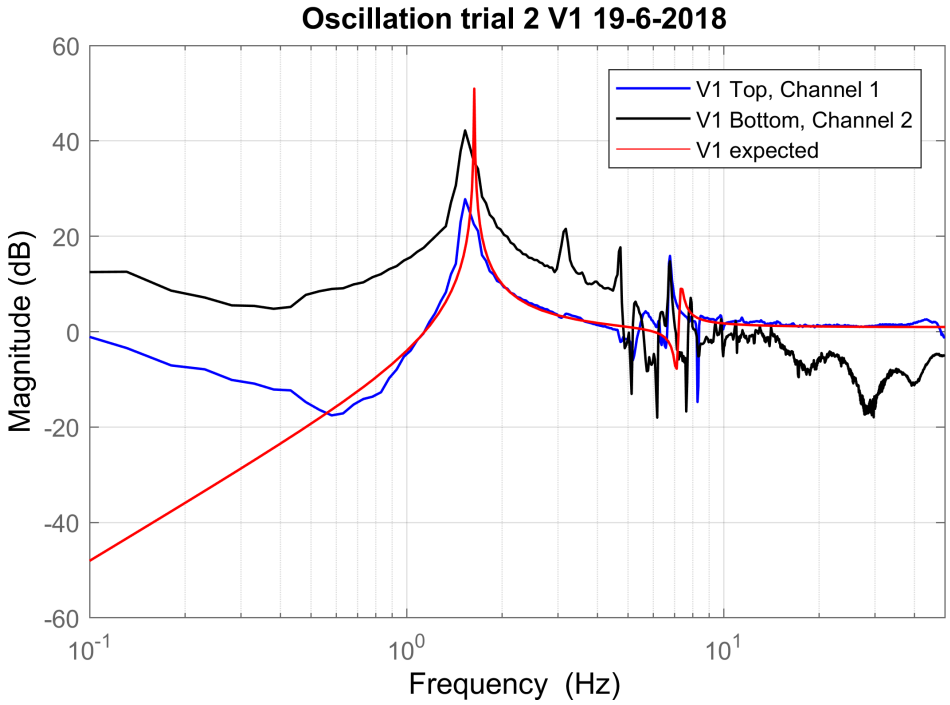

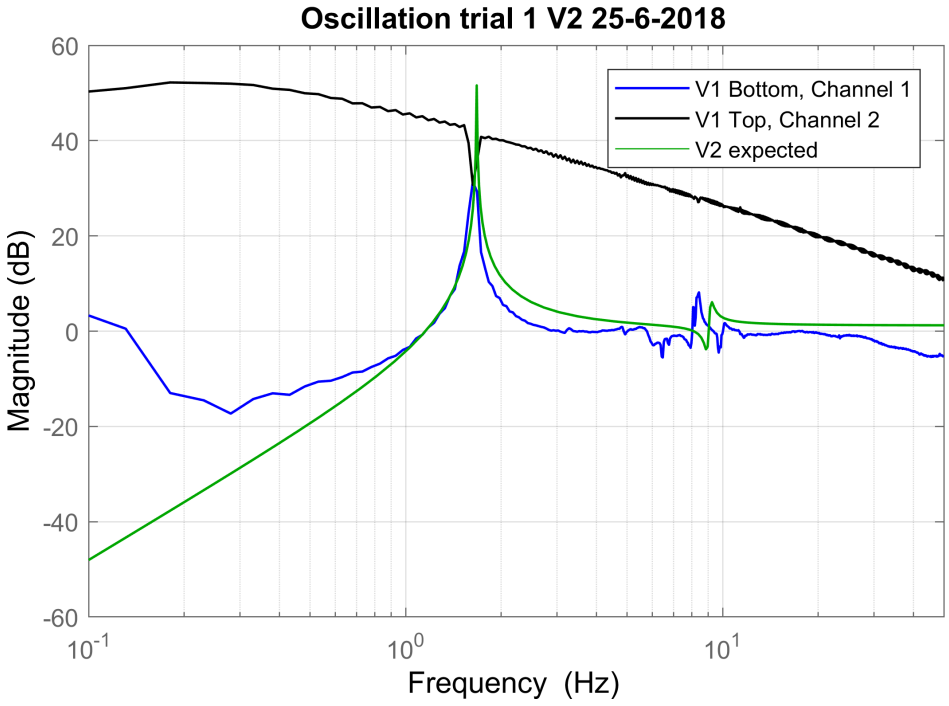
Oscillation trial 1 V2 25-6-2018
V1 Bottom, Channel 1
V1 Top, Channel 2
V2 expected
Magnitude (dB)
Frequency (Hz)
60
40
20
0
-20
-40
-60
10^-1
10^0
10^1

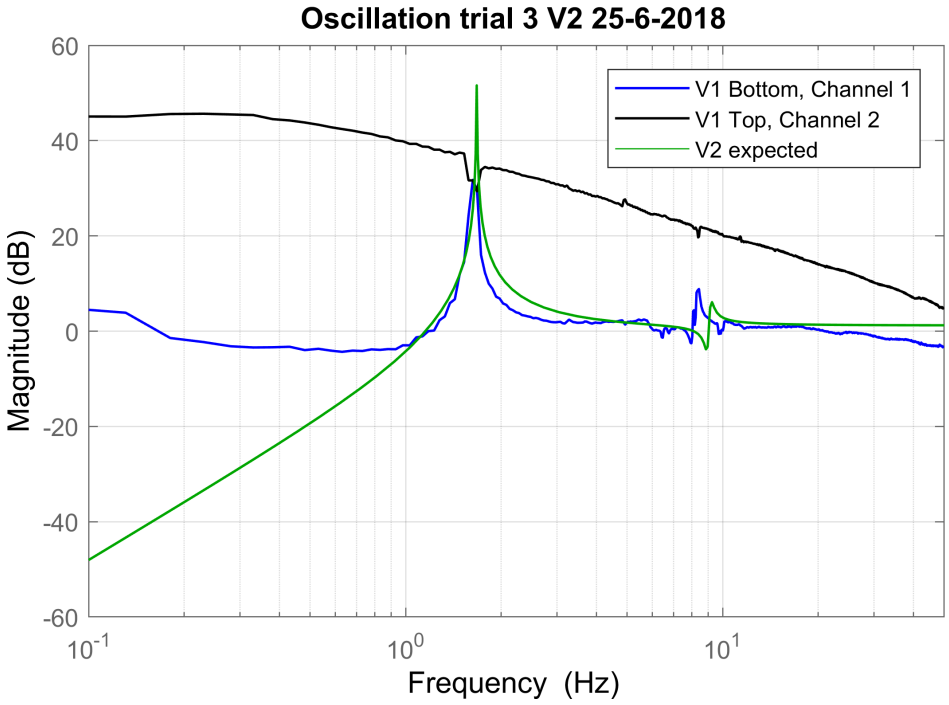
Oscillation trial 3 V2 25-6-2018
V1 Bottom, Channel 1
V1 Top, Channel 2
V2 expected
Magnitude (dB)
Frequency (Hz)
60
40
20
0
-20
-40
-60
10^-1
10^0
10^1

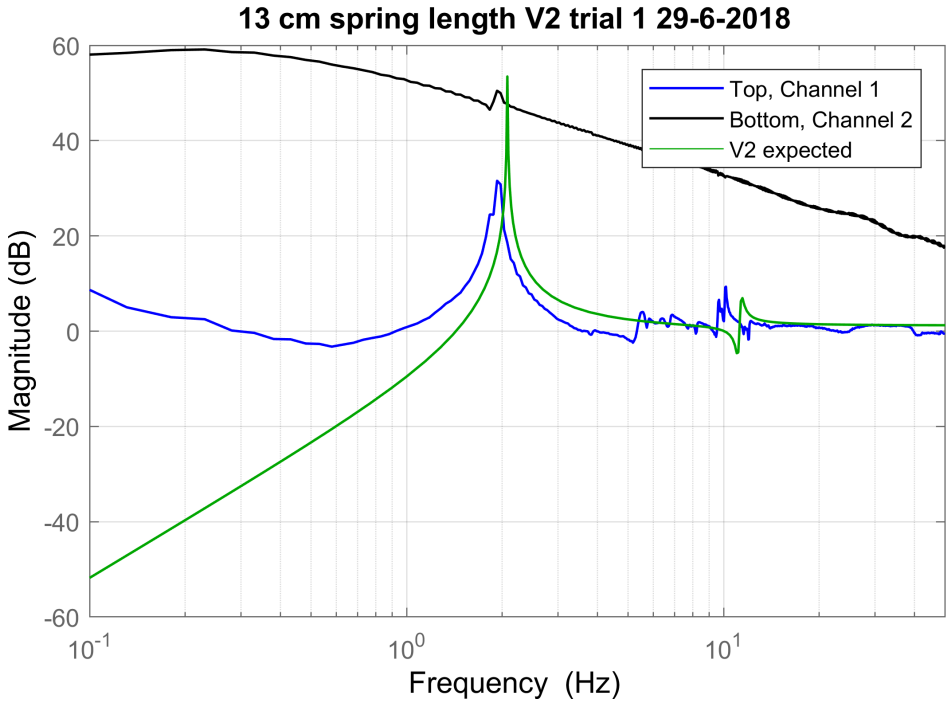
13 cm spring length V2 trial 1 29-6-2018
Top, Channel 1
Bottom, Channel 2
V2 expected
Magnitude (dB)
Frequency (Hz)
60
40
20
0
-20
-40
-60
10^-1
10^0
10^1

B.2 Pitching

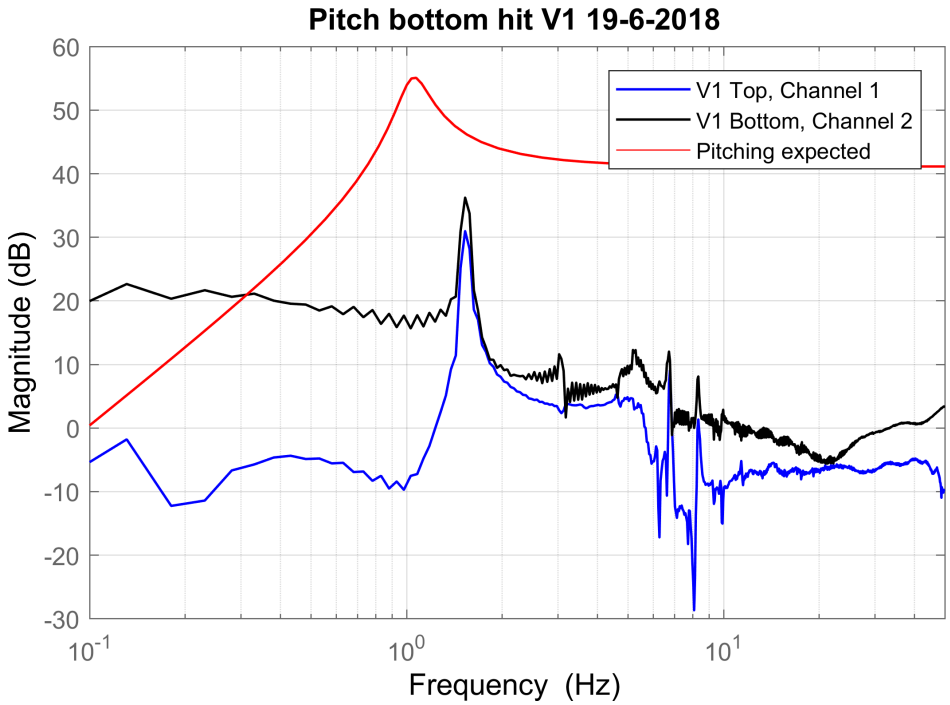
Pitch bottom hit V1 19-6-2018
V1 Top, Channel 1
V1 Bottom, Channel 2
Pitching expected
Magnitude (dB)
Frequency (Hz)
60
50
40
30
20
10
0
-10
-20
-30
10^-1
10^0
10^1

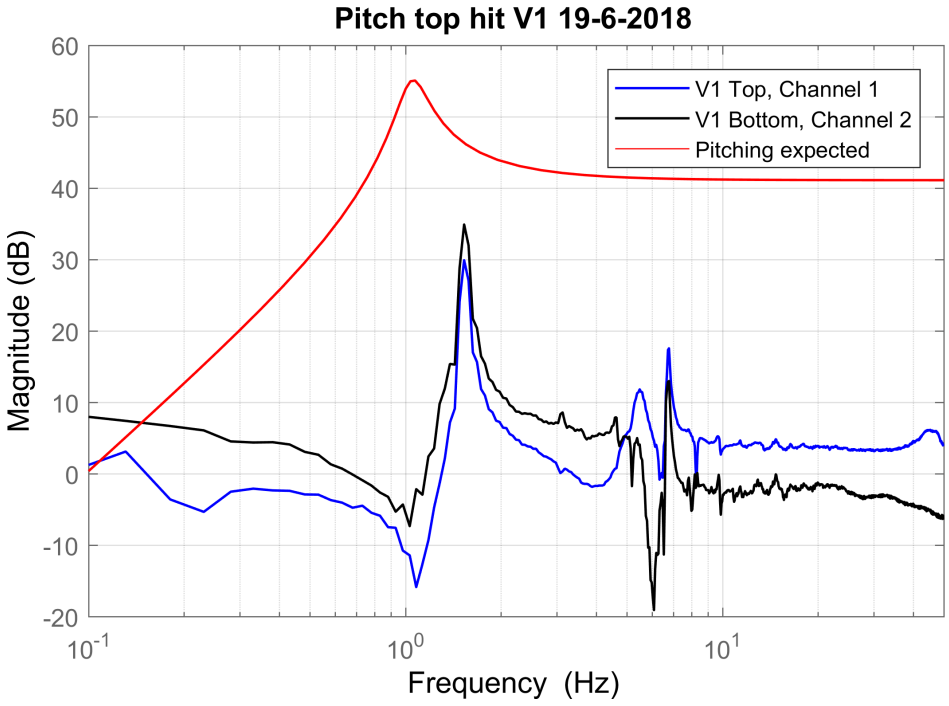
Pitch top hit V1 19-6-2018
V1 Top, Channel 1
V1 Bottom, Channel 2
Pitching expected
Magnitude (dB)
Frequency (Hz)
60
50
40
30
20
10
0
-10
-20
10^-1
10^0
10^1

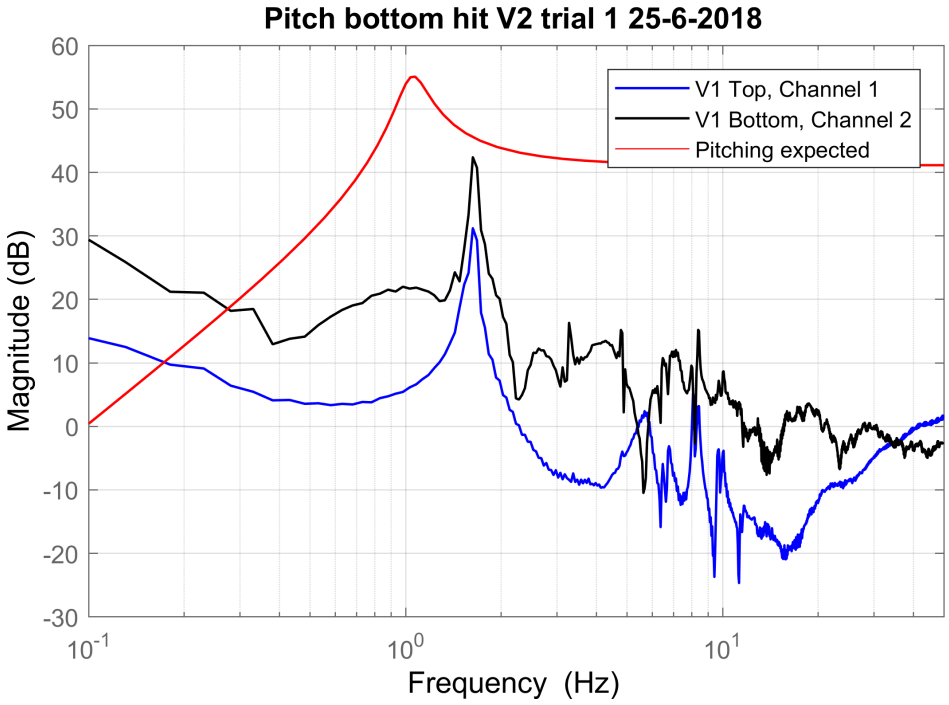
Pitch bottom hit V2 trial 1 25-6-2018
V1 Top, Channel 1
V1 Bottom, Channel 2
Pitching expected
Magnitude (dB)
Frequency (Hz)
60
50
40
30
20
10
0
-10
-20
-30
10^-1
10^0
10^1

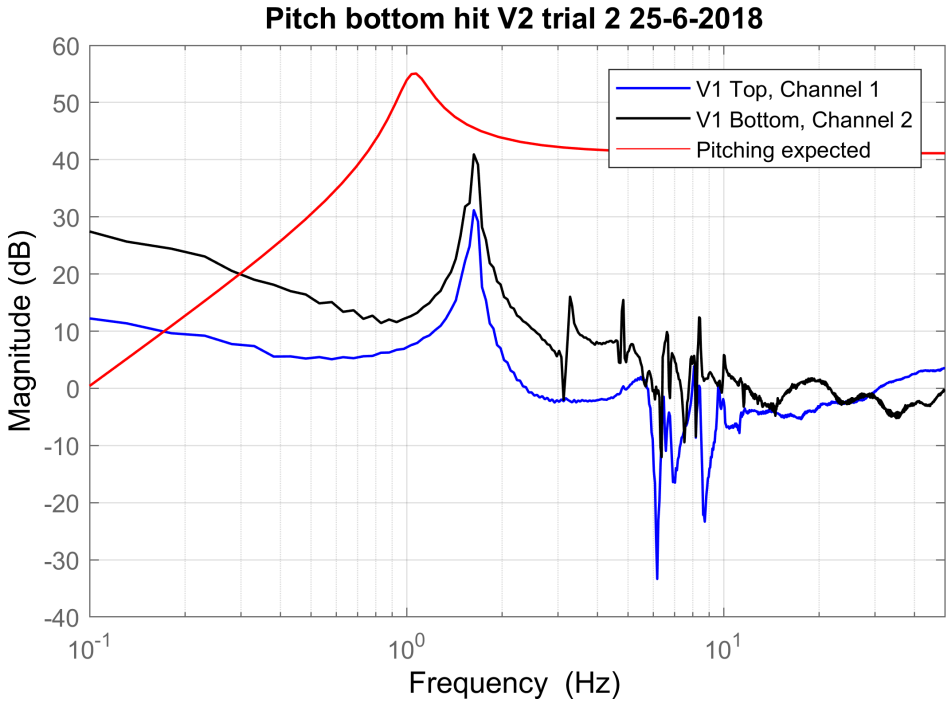
Pitch bottom hit V2 trial 2 25-6-2018
V1 Top, Channel 1
V1 Bottom, Channel 2
Pitching expected
Magnitude (dB)
Frequency (Hz)
60
50
40
30
20
10
0
-10
-20
-30
-40
10^-1
10^0
10^1

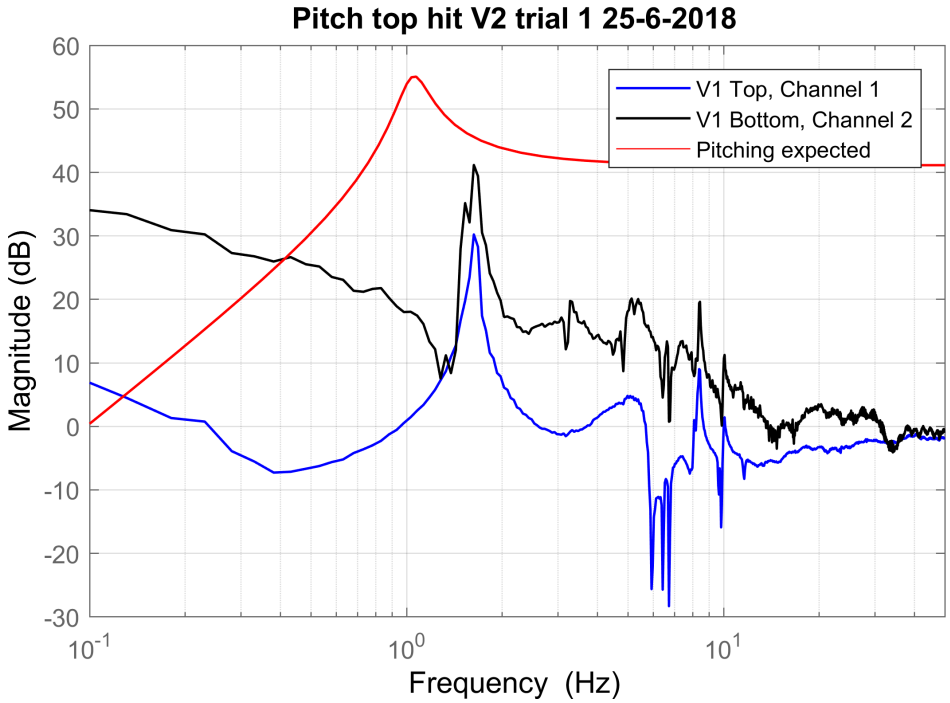
Pitch top hit V2 trial 1 25-6-2018
V1 Top, Channel 1
V1 Bottom, Channel 2
Pitching expected
Magnitude (dB)
Frequency (Hz)
60
50
40
30
20
10
0
-10
-20
-30
10^-1
10^0
10^1

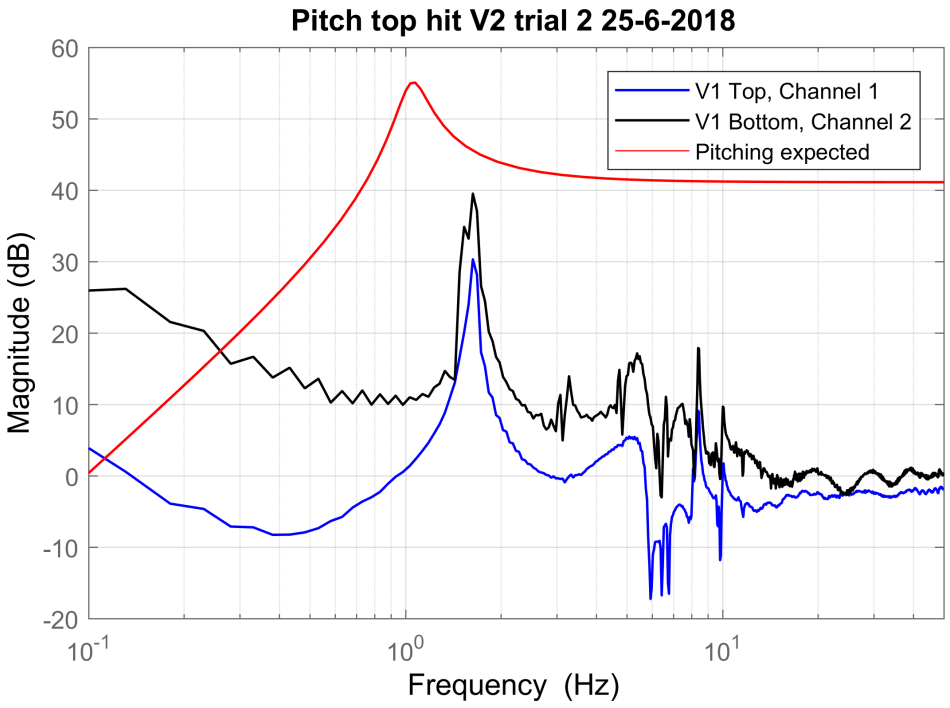

B.3 Side Blocks

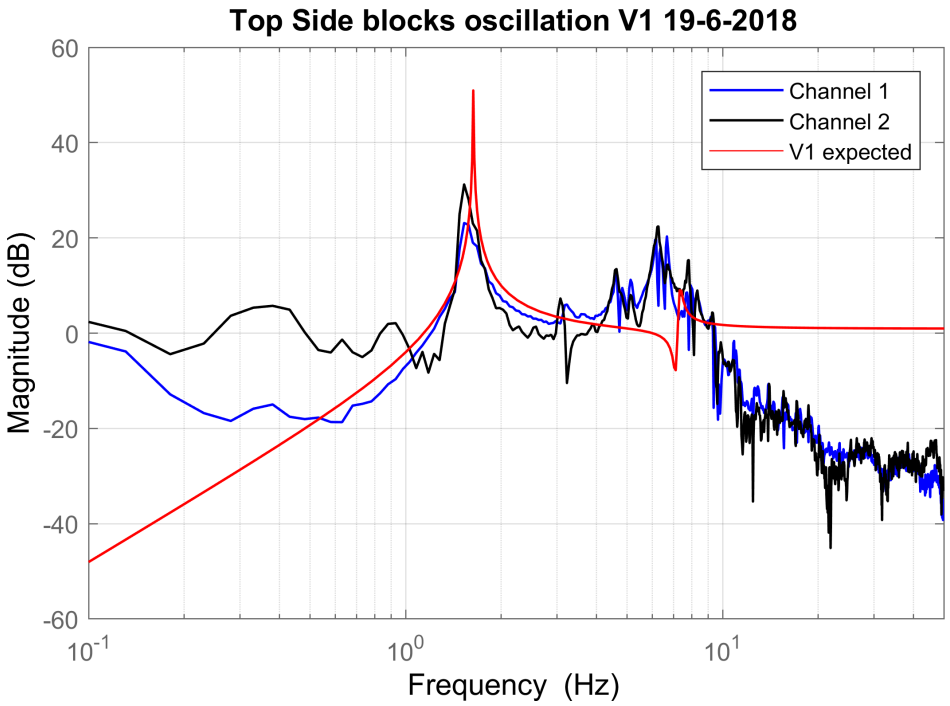

Bibliography

Adafruit (2018), Adafruit VL6180X Time of Flight micro-LIDAR Distance Sensor Breakout, date last accessed: 4/7/2018.
https://learn.adafruit.com/adafruit-vl6180x-time-of-flight-micro-lidar-distance-sensor-breakout?view=all

Allan, J. R. and A. P. Orosz (2001), The Costs of Birdstrikes to Commercial Aviation, Digital Commons, University of Nebraska.
https://digitalcommons.unl.edu/birdstrike2001/2/

Janssen Precision Engineering (2018), FLEXURE ENGINEERING FUNDAMENTAL - LEAF SPRING, date accessed: 4/5/2018.
https://www.janssenprecisionengineering.com/page/flexure-engineering-fundamental-leaf-spring/

Landman, E. (2016), *Test Rig for the Robird*, Master's thesis, University of Twente, Robotics and Mechatronics group.

MakeItFrom.com (2018), AISI 301 (1.4310, S30100) Stainless Steel, date last accessed: 6/6/2018.
https://www.makeitfrom.com/material-properties/AISI-301-1.4310-S30100-Stainless-Steel

Rosenberg, T. (2017), Where Birds and Planes Collide, a Winged Robot May Help., date accessed: 4/5/2018.
www.nytimes.com/2017/11/28/opinion/birds-planes-robird.html

Seidenman, P. (2016), How Bird Strikes Impact Engines, date accessed: 4/5/2018.
www.mro-network.com/maintenance-repair-overhaul/how-bird-strikes-impact-engines

Soemers, H. (2011), *Design Principles for Precision Mechanisms*, University of Twente, ISBN 978-90-365-3103-0.